

My, how you've grown: a practical guide to modeling size transitions for Integral Projection Model (IPM) applications

Tom E.X. Miller^{*a} and Stephen P. Ellner^b

^aDepartment of BioSciences, Rice University, Houston, TX

^bDepartment of Ecology and Evolutionary Biology, Cornell University,
Ithaca, New York

Running header: Better growth modeling for IPMs

*Corresponding author. Department of BioSciences, Rice University, Houston, TX 77005-1827. Email:
tom.miller@rice.edu Phone: 713-348-4218

¹ **Abstract**

² 1.

³ 2.

⁴ 3.

⁵ 4.

⁶ **Keywords**

7 Introduction

8 Structured demographic models – matrix and integral projection models (MPMs and
9 IPMs) – are powerful tools for data-driven modeling of population dynamics and viabil-
10 ity that are widely used in basic and applied settings. In contrast to MPMs for popula-
11 tions with discrete structure (life stage, age class, etc.), IPMs (Easterling et al., 2000) read-
12 ily accommodate populations structured by continuous state variables, most commonly
13 size. A related innovation of the IPM framework is its emphasis on regression-based
14 modeling for parameter estimation, which carries important advantages for making the
15 most of hard-won data (Ellner et al., 2022).

16 A standard workflow allows ecologists to assemble an IPM from data using famili-
17 iar statistical tools to describe growth, survival, reproduction, and other demographic
18 transitions as functions of size (Coulson, 2012; Ellner et al., 2016). The relative ease of
19 the regression-based approach, accommodating multiple covariates (e.g., environmental
20 factors, experimental treatments) and complex variance structures (e.g., random effects,
21 correlated errors), has facilitated a growing body of IPM literature that examines how
22 biotic or abiotic factors affect population dynamics (e.g., Louthan et al., 2022; Ozgul
23 et al., 2010; Schultz et al., 2017) and explores the consequences of demographic hetero-
24 geneity associated with spatial, temporal, and individual variation (e.g., Compagnoni
25 et al., 2016; Crone, 2016; Plard et al., 2018). The vital rate regressions (or “sub-models”)
26 are the bridge between the individual-level data and the population-level model and its
27 predictions; it is important to get them right.

28 Compared to other vital rates, growth is special. The regression sub-models for
29 survival and reproduction provide the expected values of those rates as functions of
30 size (we use “size” as the name for whatever continuous variable defines the population
31 structure, which could instead be immune competence, mother’s weight, etc.). However,
32 for modeling growth, the full probability distribution of subsequent size, conditioned on
33 initial size, must be defined. This distribution defines the growth ‘kernel’ $G(z', z)$ that
34 gives the probability density of any future size z' at time $t + 1$ conditional on current size
35 z at time t . Whenever survival and reproduction are size-dependent, the entire distribu-
36 tion of size transitions can strongly influence IPM predictions because this distribution
37 governs how frequently size changes are much greater or much lower than average.

38 The original template for modeling size transitions in IPMs was provided by East-
39 erling et al. 2000. They first tried simple linear regression, assuming normally dis-
40 tributed size changes with constant variance. Because the residuals from this regression
41 exhibited non-constant variance, they used a two-step approach that estimated the size-

42 dependence in the growth variance (better options soon became available, such as the
43 `lme` function in R). However, even after accounting for non-constant variance, growth
44 data may still deviate from the assumption that size transitions are normally distributed.
45 Size transitions are often skewed such that large decreases are more common than large
46 increases (Peterson et al., 2019; Salguero-Gómez and Casper, 2010), or vice versa (Stub-
47 berud et al., 2019). Size transitions may also exhibit excess kurtosis ('fat tails'), where
48 extreme growth or shrinkage is more common than predicted by the tails of the normal
49 distribution (Hérault et al., 2011).

50 The observation that the normal distribution may poorly describe size transitions
51 in real organisms has been made before, and several studies have emphasized that al-
52 ternative distributions should be explored (Easterling et al., 2000; Peterson et al., 2019;
53 Rees et al., 2014; Williams et al., 2012). Yet, default use of Gaussian growth distribu-
54 tions (often with non-constant variance) remains the standard practice. An ISI Web of
55 Knowledge search on the terms 'integral projection model ecology' (DATE) returned #
56 IPM studies published in the past decade (2010–2020), # of which assumed a Gaussian
57 growth kernel.¹ The general state-of-the-art in the literature appears to remain where it
58 was 20 or so years ago, using the default model without pausing to examine critically
59 whether or not it actually provides a good description of the data. We are guilty of this,
60 ourselves.

61 The persistence of Gaussian growth modeling is understandable. There is a long
62 tradition of statistical modeling built on the assumption of normally distributed residu-
63 als with constant variance. Popular software packages such as `lme4` (Bates et al., 2007)
64 and `MCMCglmm` (Hadfield et al., 2010) make it easy to fit growth models with po-
65 tentially complex fixed- and random-effect structures, but the possible distributions of
66 continuous responses are limited, and default to Gaussian. Abandoning these conve-
67 nient tools for the sake of more flexible growth modeling means, it may seem, sacrificing
68 the flexibility to rigorously model diverse and potentially complex sources of variation
69 in growth, some of which may be the motivation driving the study in the first place.

70 The question we address here is: how can ecologists escape the apparent trade-off
71 between realistically capturing the variance, skew, and kurtosis of size transition data
72 on the one hand, and flexibly including the multiple covariates and random effects that
73 often have substantial impacts on demographic rates. In this article, we offer an answer.

74 Our goal here is to present and illustrate a general 'recipe' that moves growth mod-
75 eling past the standards set over 20 years ago. Like any recipe, users may need to
76 make substitutions or add ingredients to suit their situation. Our approach emphasizes

¹I still intend to do this! But it's a rabbit hole I have not gone down yet.

77 graphical diagnostics for developing and evaluating growth models, rather than a pro-
78 cess centered on statistical model selection. Through a set of empirical case studies we
79 demonstrate how a simple workflow, using tools that were nonexistent or not readily
80 available when IPMs first came into use, makes it straightforward and relatively easy to
81 identify when the default model is a poor fit to the data, and to then choose and fit a
82 substantially better growth model that is no harder to use in practice. We illustrate our
83 approach by revisiting four of our own, mostly published IPM analyses that assumed
84 Gaussian growth.² In each case, the Gaussian assumption does not stand up to close
85 scrutiny. We illustrate how we could have done better, and the consequences of “doing
86 better” for our ecological inferences. All of our analyses may be reproduced from code
87 and data that are publicly available (see Data accessibility statement).

88 A general workflow for better growth modeling

89 The modeling workflow that we suggest runs as follows (Fig. 1):

- 90 1. *Fit a “pilot” model or models assuming a Gaussian distribution but allowing for non-*
91 *constant variance.*

92 This step is familiar to most IPM users, as it is the start and end of the traditional
93 workflow. A well-fitted Gaussian model accurately describes the mean and variance
94 of future size conditional on current size and possibly on other measured covariates
95 or random effects. This step may include model selection to identify which treat-
96 ment effects or environmental drivers affect the mean and/or variance of future size.
97 Non-constant variance is often fitted in a two-stage process, first fitting mean growth
98 assuming constant variance, then doing a regression relating the squared residuals
99 from the initial fit to the fitted mean. It is sometimes better to fit size-dependence
100 in the mean and variance simultaneously, as can be done with the R packages **mgcv**
101 and **nmle**, because incorrectly assuming constant variance can affect the outcome of
102 model selection for the mean. One-step fitting is straightforward for simple models
103 in which initial size is the only factor that can influence growth variance. However,
104 the two-step process fitting residuals to the fitted value (expected future size) may
105 be convenient when there are multiple fixed and random effects, all of which may
106 contribute to non-constant variance, since the expected value implicitly accounts for
107 all of them. We illustrate both one-step and two-step approaches in the examples
108 below.

²Need to commit to case study choices - Steve wanted to include corals for contrast with Peterson et al.

109 Allowing non-constant variance means that it is not necessary to transform the
110 data in a way that stabilizes the growth variance. Transformation remains an option
111 when it does not create new problems (see Discussion), and it may have advantages
112 besides variance stabilization. In particular log-transformation is often appropriate
113 for size data (Ellner et al., 2016), and it helps avoid eviction at small sizes.

- 114 2. *Use statistical and graphical diagnostics to identify if and how the standardized residuals*
115 *deviate from Gaussian, and to identify a more appropriate distribution.*

116 If the Gaussian pilot model is valid, the set of standardized residuals (standardized
117 by the standard deviation) should be Gaussian with mean zero and unit variance,
118 with no skew or excess kurtosis. This criterion provides a straightforward test for
119 whether to accept a Gaussian growth model or explore alternatives. If the standard-
120 ized residuals are satisfactorily Gaussian, skip to the final step of the workflow.

121 There are many ways that growth data may deviate from Gaussian, and the
122 nature of those deviations can guide the search for a better distribution. Frequentist
123 tests such as the D'Agostino test of skewness (D'Agostino, 1970) and the Anscombe-
124 Glynn test of kurtosis (Anscombe and Glynn, 1983) could be used to diagnose
125 whether the aggregate distribution of standardized residuals deviates from normal-
126 ity (R package **moments** (Komsta and Novomestky, 2015)). However, the aggregate
127 distribution of standardized residuals may be misleading if properties such as skew
128 and kurtosis vary with size. For example, a change in the direction of skewness from
129 small to large sizes would require a distribution flexible enough to accommodate
130 both positive and negative skew, such as the skewed normal or Johnson S_U distri-
131 butions. Alternatively, growth data may lack skew but may exhibit leptokurtosis (in
132 which case the t distribution may be a good choice) or may shift from platykurtos-
133 sis to leptokurtosis depending on initial size (in which case the power exponential
134 distribution may be a good choice). It is therefore essential to visualize trends in dis-
135 tribution properties with respect to size, either initial size (for simple models with
136 only size-dependence) or expected future size (for models with multiple fixed ef-
137 fects). In the case studies below, we rely on quantile regression of the standardized
138 residuals to visualize skew and kurtosis as continuous functions of size or expected
139 value. Fig. 1 includes guidance on how the skew and kurtosis properties of the stan-
140 dardized residuals suggest options for an appropriate growth distribution. In our
141 case studies we take advantage of the many distributions provided in the **gamlss** R
142 package (Stasinopoulos et al., 2007), but any other distributions with the necessary
143 properties can be used.

144 3. *Refit the growth model using the chosen distribution.*

145 In models with multiple covariates and/or random effects, each potentially affecting
146 several distribution parameters (location, scale, skew, kurtosis) in different ways,
147 “refit the model” could entail a massive model selection process to identify the
148 “right” or “best” non-Gaussian model. And with so many options, model uncer-
149 tainty may be overwhelming and over-fitting becomes a significant risk even if pre-
150 cautions against it are taken. We therefore argue for adopting the more modest
151 goal of remedying the apparent defects in the Gaussian model. Conveniently, as
152 we demonstrate below, the functional forms for the mean and standard deviation
153 (or location and scale parameters) could be carried over from the pilot Gaussian
154 model into a non-Gaussian distribution, leaving skew and kurtosis as the targets for
155 improvement. This step exploits the fact that parameter estimation from a Gaus-
156 sian model is generally robust to deviations from normality (Schielzeth et al., 2020),
157 meaning that the mean of the Gaussian model is probably a good proxy for the mean
158 of the non-Gaussian model (and in case it is not, the next step in the workflow would
159 catch that). The functional forms for skew and kurtosis of the non-Gaussian model
160 can be guided by the qualitative features of the graphical diagnostics (e.g., skewness
161 switches from positive to negative with size).

162 4. *Test the final model through graphical diagnostics comparing simulated and real growth data.*

163 A good model will generate simulated data that look like the real data. Again, it is
164 important to inspect the properties of simulated data conditional on present size or
165 expected future size, rather than examining the entire distribution. We provide ex-
166 amples below of informative comparisons between simulated and real data, based
167 mainly on quantiles. If the simulated data do not correspond well with real data,
168 alternative (possibly more flexible) growth distributions should be explored, or more
169 complex functions relating distribution parameters to current size and other covari-
170 ates. However, we again caution against launching a full-blown model selection
171 exercise. Instead, possible alternative models could be chosen primarily to remedy
172 observable discrepancies between the real and simulated size transition data, and at
173 most slightly modified based on final diagnostic and statistical tests.

174 How should skewness and kurtosis be measured?

175 “Improvement” of a Gaussian model will always involve scrutiny of skewness and kur-
176 tosis, so measurement of these properties warrants some attention. The standard mea-

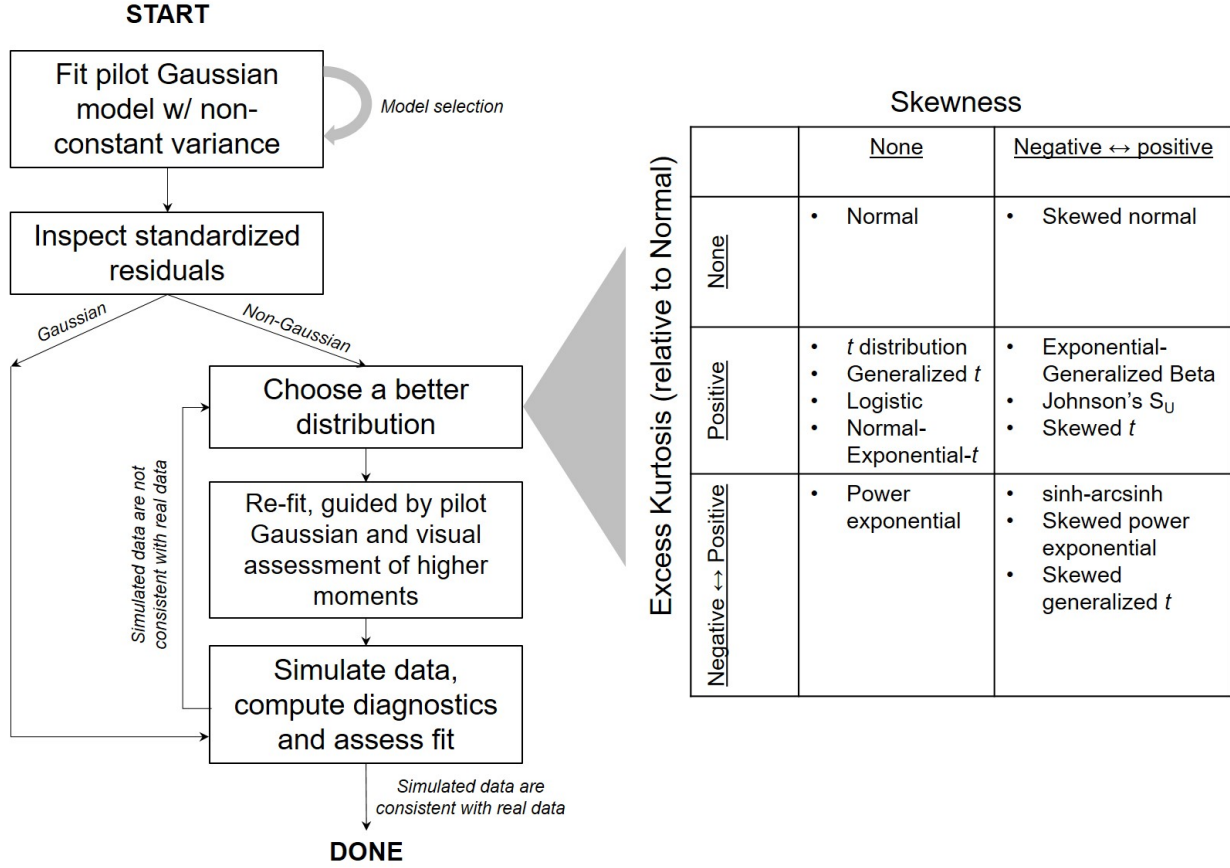


Figure 1: General workflow of recommendations for IPM growth modeling (left) and guide to common non-Gaussian distributions of size x for $x \in \mathbb{R}$ that can accommodate different combinations of skewness and kurtosis (right). All of these distributions (often including multiple versions or parameterizations of each) are available in the package **gamlss.dist**, except for the skewed generalized *t*, which is available in the package **sgt** (Davis, 2015).

¹⁷⁷ sures of skewness and kurtosis (tail thickness) are based on the third and fourth central
¹⁷⁸ moments, respectively, of the distribution:

$$\text{Skewness} = \frac{m_3}{\sigma^3}, \quad \text{Excess kurtosis} = \frac{m_4}{\sigma^4} - 3 \quad (1)$$

¹⁸⁰ where $m_k = \mathbb{E}(X - \bar{X})^k$ is the k^{th} central moment of a random quantity X and σ^2 is the
¹⁸¹ variance (second central moment). A Gaussian distribution has zero skewness and zero
¹⁸² excess kurtosis.

¹⁸³ The standard measures are easy to calculate but their use for choosing and eval-
¹⁸⁴ uating growth models is hindered by their poor sampling properties. Because empirical
¹⁸⁵ estimates involve high powers of data values, it only takes a few outliers to produce



Figure 2: Histograms of skewness and kurtosis estimates using moment-based definitions, compared with the nonparametric measures. Histograms are based on 5000 replicate draws of a sample of 200 independent values from a t distribution with 8 degrees of freedom. Dotted red vertical lines mark the minimum and maximum of sample estimates, and dashed blue lines show the 5th and 95th percentiles. The true value is indicated by a black dot on the x -axis. Figure drawn by script `NPmoments.R`

186 a very inaccurate estimate. Figure 2 shows a simulated example, where the underlying
 187 “data” are a sample of size 200 from a t distribution with 8 degrees of freedom; the true
 188 skew is 0, and the true excess kurtosis is 1.5. The distance between the largest and small-
 189 est estimates (indicated by the dotted red vertical lines), relative to the distance between
 190 the 5th and 95th percentiles, shows the broad extent of extreme values that can occur
 191 even with a good size sample, especially for kurtosis.

192 We therefore use “nonparametric” (NP) measures of skew and kurtosis that are
 193 based on quantiles and thus less sensitive to a few extreme data values. Let q_α denote
 194 the α quantile of a distribution or sample (e.g., $q_{0.05}$ is the 5th percentile). For any
 195 $0 < \alpha < 0.5$, a quantile-based measure of skewness is given by (McGillivray, 1986)

$$196 \text{NP Skewness} = \frac{q_\alpha + q_{1-\alpha} - 2q_{0.5}}{q_{1-\alpha} - q_\alpha}. \quad (2)$$

197 NP Skewness is a measure of asymmetry between the tails of the distribution above and
 198 below the median. The size of the upper tail can be measured (for any $0 < \alpha < 0.5$) by
 199 $\tau_U = q_{1-\alpha} - q_{0.5}$; for $\alpha = 0.05$ this is the difference between the 95th percentile and the
 200 median. The lower tail size is $\tau_L = q_{0.5} - q_\alpha$. The definition above is equivalent to

$$201 \quad \text{NP Skewness} = \frac{\tau_U - \tau_L}{(\tau_U + \tau_L)}. \quad (3)$$

202 So an NP Skewness of ± 0.2 says that the difference in tail sizes is 20% of their total. The
 203 range of possible values is -1 to 1. Both $\alpha = 0.25$ (sometimes called “Kelly’s skewness”)
 204 and $\alpha = 0.1$ (“Bowley’s skewness”) are common choices. We used $\alpha = 0.1$, unless
 205 otherwise stated.

206 An analogous quantile-based measure of kurtosis (Jones et al., 2011) is

$$207 \quad \text{NP Kurtosis} = \frac{q_{1-\alpha} - q_\alpha}{q_{0.75} - q_{0.25}}. \quad (4)$$

208 For $\alpha = 0.05$, NP Kurtosis is the difference between the 95th and 5th percentiles, relative
 209 to the interquartile range. To facilitate interpretation, we scale NP Kurtosis relative to
 210 its value for Gaussian distribution, and subtract 1. We call this “NP Excess Kurtosis”.
 211 The value for a Gaussian distribution is zero. A value of 0.2 means that the tails are (on
 212 average) 20% heavier than those of a Gaussian with the same interquartile range, and
 213 a value of -0.2 means that the tails are (on average) 20% lighter than a Gaussian with
 214 the same interquartile range. We calculate NP Kurtosis using $\alpha = 0.05$ unless otherwise
 215 stated, to focus on the tail edges, but again this is somewhat arbitrary.

216 Figure 2C,D illustrate how, applied to exactly the same simulated samples, the non-
 217 parametric measures of skewness and kurtosis produce a smaller fraction of highly in-
 218 accurate estimates caused by a few extreme values in the sample. But also note that, in
 219 contrast to the moment-based measures, numerically small values of the NP measures
 220 (e.g., 0.1 or 0.2) should not be disregarded, because they are both scaled so that a value
 221 of 1 indicates extremely large departures from a Gaussian distribution.

222 Quantile-based estimation of skewness and kurtosis carries the added value that
 223 quantile regression methods may be used to derive these properties of size transitions
 224 as continuous functions of initial size or expected future size. In the examples below,
 225 we use the **qgam** package to fit smooth additive quantile regression models, which have
 226 the flexibility to accommodate non-linear size-dependence in skewness and kurtosis.
 227 One risk of a gam-based approach is that fitted quantiles may be too “wiggly” without
 228 constraints on their complexity (in the examples below, we specify $k = 4$ to constrain the

dimension of the basis function). For the gam-averse, other quantile regression models may be equally suitable. For consistency with non-parametric skewness and kurtosis, we similarly use quantile-based measures of mean and variance and quantile regression to visualize these as functions of size. Specifically, following Wan et al. (2014),

$$\text{NP Mean} = \frac{q_{0.25} + q_{0.5} + q_{0.75}}{3} \quad (5)$$

and

$$\text{NP SD} = \frac{q_{0.75} - q_{0.25}}{1.35}. \quad (6)$$

1 Case study: Sea fan corals, *Gorgonia ventalina*

We begin with a simple example where current size is the only predictor of future size. Bruno et al. (2011) developed an IPM to understand the rise and fall of a fungal pathogen *Aspergillus sydowii* in Caribbean sea fan corals *G. ventalina*. The model was based on repeated observations of marked corals in permanent transects at several sites near Akumal, Mexico, recording disease status (infected/uninfected) and the area of uninfected tissue. The epidemic peak had passed and disease incidence was already low, so infected fans were relatively infrequent. We therefore limit the analysis here to uninfected individuals. Bruno et al. (2011) found statistically significant year and site effects, but as those explained a very small fraction of the variation in growth increments, they fitted a single growth model to data pooled across years and sites. We do the same here. The pooled data set consists of 358 observed size transitions. The data exhibited size-dependent variance in growth (change in area, cm^2), which Bruno et al. (2011) chose to stabilize by transforming size, using the cube-root of total fan area as the size measure (fig. ??B), and then fitting the standard model with Gaussian growth increments. Here we take a different approach, modeling size-dependent variance explicitly rather than trying to transform it away.

We develop a model using natural log transformation of area. With initial size as the only predictor, a simple way to fit a Gaussian model with nonconstant variance is the `gam` function in `mgcv` library (Wood, 2017) using the `gaulss` family. The mean and standard deviation are both fitted as smoothing spline functions of initial size, and the `predict` function returns the fitted mean and also the inverse of the fitted standard deviations with which we can compute the scaled residuals:

```
# XH is a data frame holding the data
# logarea.t0, .t1 denote initial and final values of log-transformed area
```

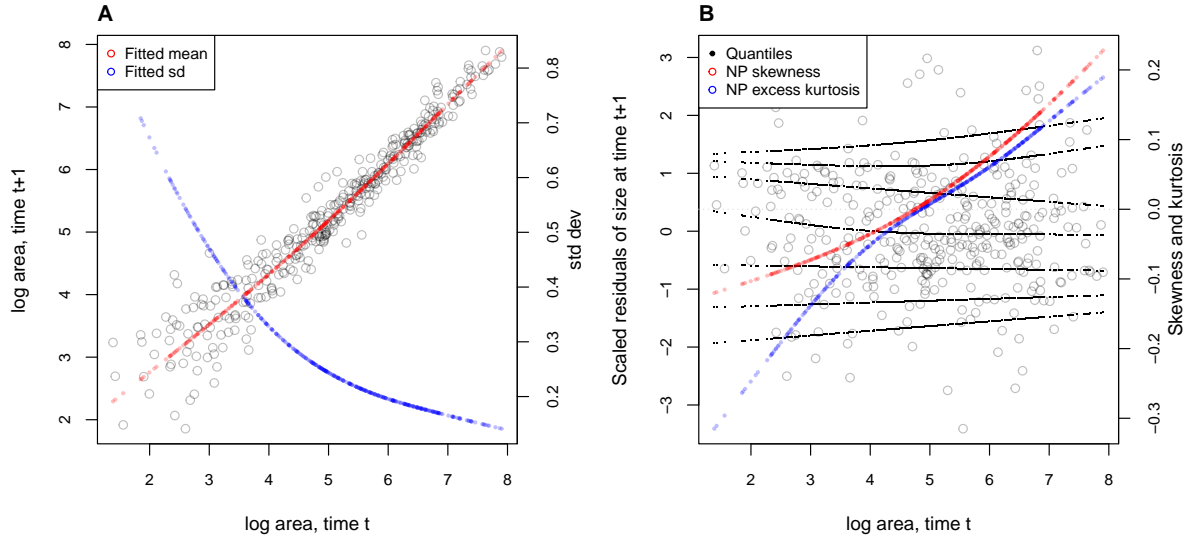


Figure 3: **A**, Size transition data for sea fan corals, *Gorgonia ventalina*, and fitted gam with mean (red) and standard deviation (blue) of future size conditional on current size. **B**, Quantile regressions of scaled residuals on size and nonparametric estimates of skewness (red) and excess kurtosis (blue) derived from them. Black lines in **B** show the 5th, 10th, 25th, 50th, 75th, 90th, and 95th quantiles. Figure made by script AkumalCorals_qgam.R.

```

261 fitGAU <- gam(list(logarea.t1~ s(logarea.t0), ~ s(logarea.t0)),
262   data=XH, gamma=1.4, family=gaulss())
263 fitted_all = predict(fitGAU,type="response");
264 fitted_sd = 1/fitted_all[,2];
265 scaledResids = residuals(fitGAU,type='response')/fitted_sd;

```

Fig. 3A shows the log-transformed data and Gaussian model. The mean function (solid blue curve) is visually nearly linear, but the fitted nonlinear spline is strongly favored over a linear model for the mean ($\Delta AIC \approx 9$). The spline for standard deviation σ versus initial size shows that smaller individuals exhibit greater variability in future size.

There are no blatant signs of trouble in the pilot Gaussian model, but quantile regressions on the scaled residuals, and the NP Skewness and Kurtosis metrics derived from them (Eq. 3 and 4), suggest deviations from normality (Fig. 3B). Specifically, skewness switches from negative to positive across the size distribution, with smaller corals more likely to shrink than grow and larger corals more likely to grow than shrink. Kurtosis also changes direction over the size distribution, with smaller initial sizes having thinner tails and larger initial sizes having fatter tails than Gaussian. The fitted nonparametric moments suggest that the upper and lower tails of size transition proba-

278 bilities may differ by up to 20%, and the weight of the tails may be 20% greater or less
279 than Gaussian, depending on initial size – not overwhelming deficiencies, but not trivial
280 either. Are these deviations from normality severe enough to warrant a second, non-
281 Gaussian iteration of growth modeling? This question may be answered by simulating
282 data from the Gaussian model and examining whether key properties of the simulated
283 data are consistent with those of the real data – this is the ultimate litmus test for a
284 growth model’s adequacy and should be a standard element of IPM construction, in our
285 opinion. If the simulated data are not consistent with the real data, it is time to choose
286 a better distribution (Fig. 1). In this case, the negative skew at small sizes and excess
287 kurtosis observed at large sizes are more extreme than what occurs across 100 random
288 iterations of data simulation (Fig. 4), suggesting that, for at least some parts of the size
289 distribution, a non-Gaussian model would better capture size transitions.

290 We sought a distribution that could accommodate the properties of the scaled resid-
291 uals, specifically changes in the sign of skewness and excess kurtosis across initial sizes.
292 We chose the sinh-arcsinh (SHASH) distribution, a four-parameter distribution that, con-
293 veniently, is included in **mcmc**’s **gam()** function:

```
294 fitSHASH <- gam(list(logarea.t1 ~ s(logarea.t0,k=4), # <- location  
295 ~ s(logarea.t0,k=4), # <- log-scale  
296 ~ s(logarea.t0,k=4), # <- skewness  
297 ~ s(logarea.t0,k=4)), # <- log-kurtosis  
298 data = XH, family = shash, optimizer = "efs")
```

299 Data simulated from this model are more consistent with the real data than the Gaussian
300 model: many of the 100 simulated SHASH data sets exhibited negative skew at small
301 sizes and positive excess kurtosis at large sizes that were as strong or stronger than
302 observed in the real data (Fig. 4). If one cared to quantify the difference between models,
303 the SHASH is clearly favored by AIC despite having twice as many parameters as the
304 Gaussian ($\Delta AIC = 7.04$).

305 What, then, have we gained by fitting a better growth model? Fig. 5A compares
306 the predicted distributions of subsequent size in the fitted model and Gaussian pilot
307 models, for the median size of a new recruit (leftmost pair of curves), the median initial
308 size (central curves), and the 95th percentile of initial size in the data (rightmost curves).
309 The differences are small, and most pronounced for the smallest size, where recruits
310 are predicted to grow slightly larger under the SHASH model than the Gaussian model.
311 The direction of this difference was surprising, since the SHASH accommodates negative
312 skew at small sizes in the data. However, in modeling skew appropriately, the SHASH

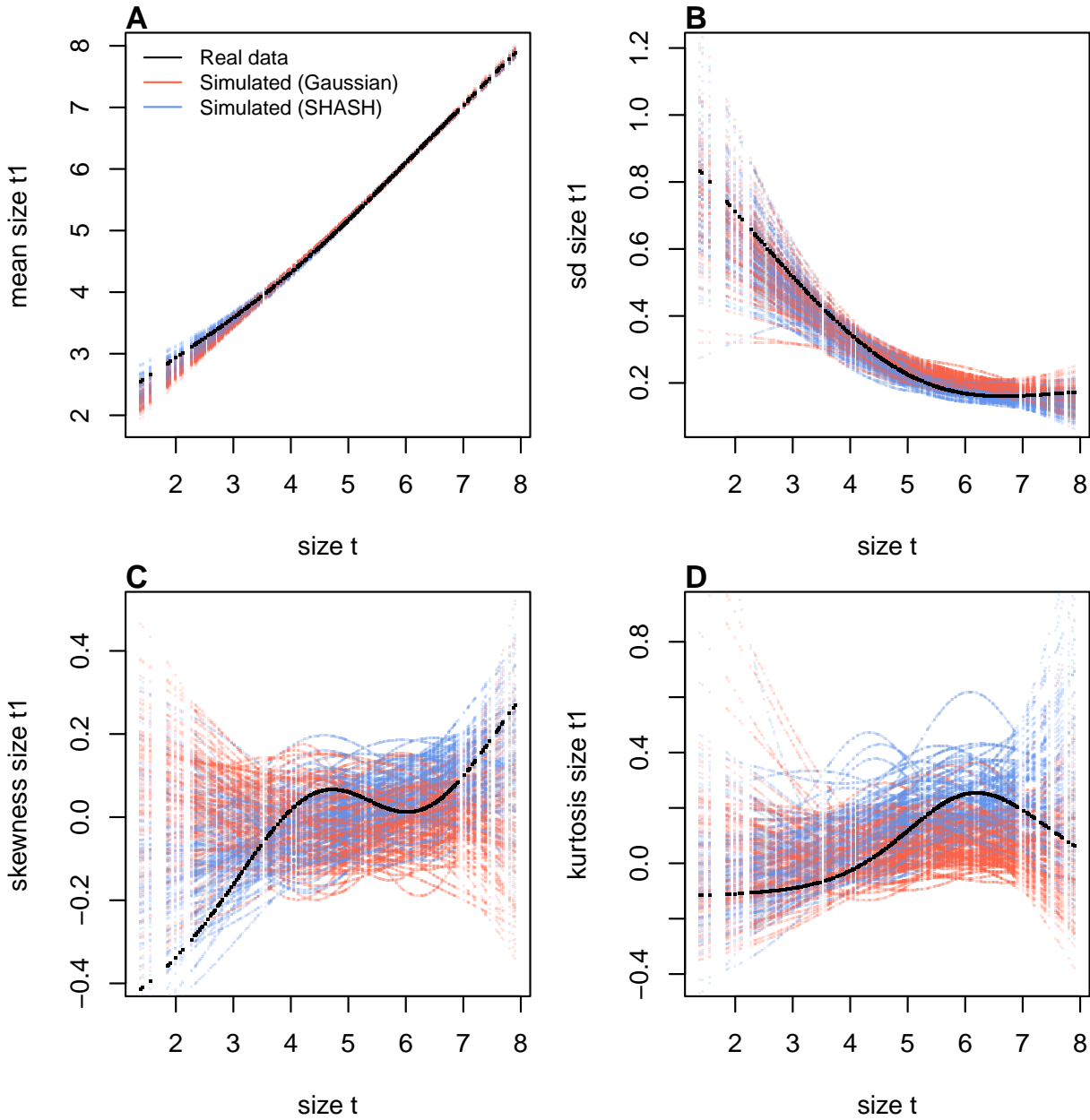


Figure 4: Comparisons among real coral data and data simulated from Gaussian and SHASH growth models for mean, standard deviation, NP skewness, and NP kurtosis of future size conditional on current size. Figure made by script `AkumalCorals_qgam.R`.

model also gives a better prediction for mean growth at small sizes than the Gaussian model, whose mean is biased downward by negative skew (Fig. 4A)³. Something similar happens in the standard deviation at large sizes (log size 5–7), where excess kurtosis in the data biased the SD upward (Fig. 4B). Fig. 5B shows the predicted steady-state size

³...Contradicting the earlier assertion that parameter estimates from Gaussian models are robust to deviations from normality!

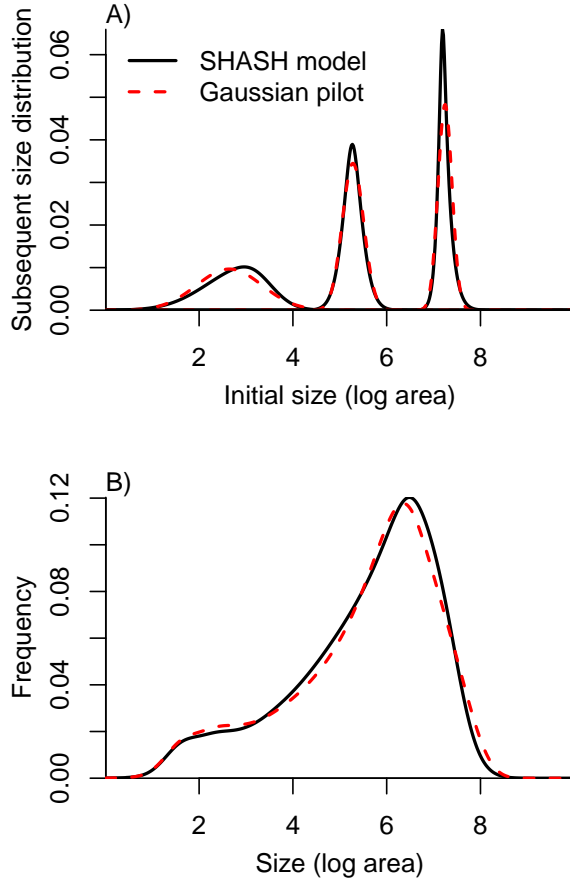


Figure 5: Comparisons between the fitted SEP1 growth model (solid black curves) and the Gaussian pilot model (dashed red curves) for sea fans *G. ventalina*. A) Predicted frequency distributions of size in year $t + 1$ for three different values of size in year t . The leftmost pair of curves are for initial size equal to the median size of a new recruit (data from (Bruno et al., 2011)); central pair is for the median initial size of uninfected individuals; rightmost pair are for the 95th percentile initial size for uninfected individuals. B) Steady-state size distributions resulting from a constant unit input of new recruits. As in Bruno et al. (2011) we assume that larvae are very widely dispersed, so that the number of recruits arriving at any one location is independent of the local population abundance or structure. Size distribution of recruits was described by a kernel density estimate based on the (sadly, only $n = 9$) measured sizes of known new recruits. Figure made by script AkumalCoralsIPMs.R.

317 distributions resulting from a constant unit input of recruits. Again, the differences are
 318 very subtle. Finally, the Gaussian and SHASH growth models predict very similar mean
 319 life span (17.7 and 17.9 years, respectively). From these outputs, there is little evidence
 320 that improved modeling of coral growth meaningfully improved biological inferences
 321 from the IPM; one could argue that it was not worth the trouble.

322 In this case study we used `gam` to fit both the Gaussian and SHASH models because
323 that obviated model selection on functions for mean, variance, and higher moments.
324 However, `gam` should be used with caution. Nonparametric regression models notori-
325 ously “wag their tails” because the ends of the fitted curve can be pulled close to the
326 outermost data points. This is especially problematic for growth modeling, because data
327 are typically sparse near the bounds of the size distribution. To minimize the risk of
328 overfitting we specified the number of “knots” (`k=4`) and used `gamma=1.4` to overweight
329 model degrees of freedom, as suggested by Gu (2013, sec. 3.2). But it is always impor-
330 tant to plot the fitted splines and make sure they do not wag unrealistically. If they do,
331 parametric regression may be a better choice.

332 2 Case study: tree cholla cactus, *Cylindriopuntia imbricata*

333 The next case study, focusing on the tree cholla cactus *Cylindriopuntia imbricata* at the
334 Sevilleta Long-Term Ecological Research site in central New Mexico, adds a new feature
335 on top of the simple size-dependent regressions in the previous study: random effects
336 associated with temporal (year) and spatial (plot) environmental heterogeneity. This
337 long-term study of cactus demography was initiated in 2004 and different subsets of
338 the data have been analyzed in various IPM studies, all using Gaussian growth kernels
339 (Compagnoni et al., 2016; Czachura and Miller, 2020; Elderd and Miller, 2016; Miller
340 et al., 2009; Ohm and Miller, 2014). In fact, (Elderd and Miller, 2016) presented a Gaus-
341 sian growth model fit to the cactus data as an example of a well fit growth function,
342 based on a marginal distribution of residuals that appeared approximately Gaussian
343 and posterior predictive checks (PPCs) of a Bayesian model that suggested consistency
344 between the real data and data simulated from the fitted model (Fig. 4 in (Elderd and
345 Miller, 2016)). While PPCs and the associated “Bayesian P-value” are popular diagnostic
346 tools, they are often considered to be too conservative (Conn et al., 2018; Zhang, 2014),
347 failing to reject marginally bad models even though they are very effective in rejecting
348 models that are terrible. The choice of discrepancy function (the statistic used to com-
349 pare real and simulated data) can also be limiting: in our previous work, we used a
350 discrepancy function focused on variance (the sum of the squared residuals), so we had
351 a built-in blind-spot for mismatches in higher moments. In the clarity of hindsight, the
352 PPC gave a false sense of security; the Gaussian was a poor choice all along.

353 The data for this new analysis include 4844 size transition observations from 929 in-
354 dividuals spanning 13 transition years (2004–2018) and 11 spatial replicates (three spatial
355 blocks in years 2004–2008 and eight 30m-by-30m plots in years 2009–2018). The data are
356 provided in Miller (2020). Following previous studies, we quantified size as the natural
357 logarithm of plant volume (cm^3), derived from height and width measurements.

358 We begin the growth modeling workflow, as above, with a generalized additive
359 model with the mean and standard deviation of size in year $t + 1$ modeled as function
360 of size in year t , with random intercepts for year and plot and assuming normally dis-
361 tributed residuals (`family=gaulss()`). The standardized residuals, accounting for size-
362 dependent residual variance (Fig. 6A), show clear signals of negative skew and positive
363 excess kurtosis across most of the size distribution but strongest in the middle of the size
364 distribution (Fig. 6B).

365 To better capture size transitions, we need a distribution with negative skew and
366 positive excess kurtosis, but both of which may be negligible at some sizes. We first tried

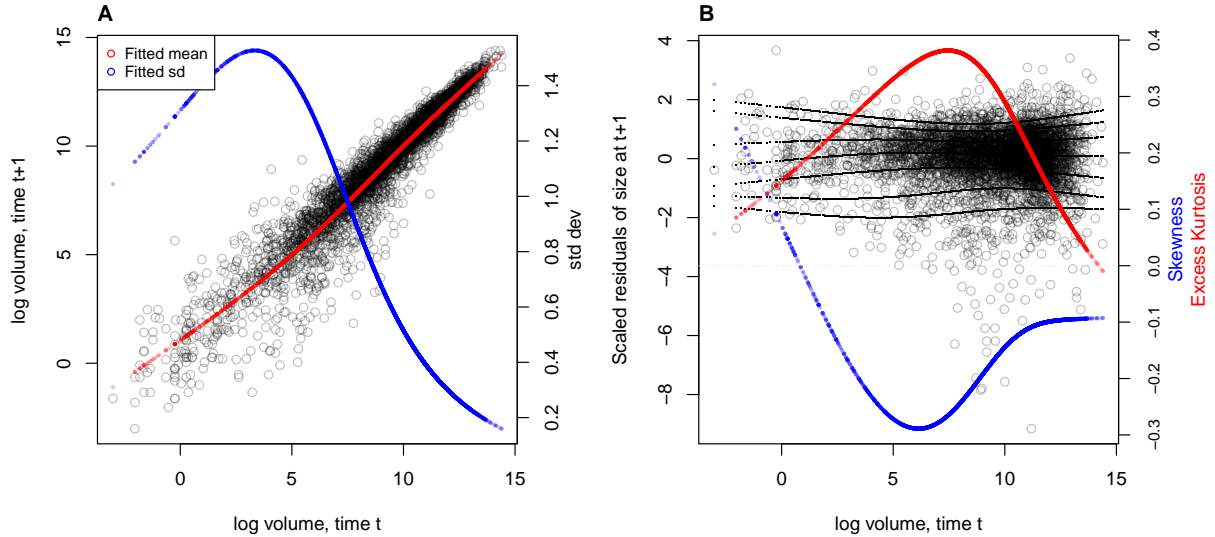


Figure 6: **A**, Size transition data for tree cholla cacti, *Cylindropuntia imbricata*, and fitted gam with mean (red) and standard deviation (blue) of future size conditional on current size. **B**, Quantile regressions of scaled residuals on size and nonparametric estimates of skewness (red) and excess kurtosis (blue) derived from them. Black lines in **B** show the 5th, 10th, 25th, 50th, 75th, 90th, and 95th quantiles. Figure made by script `cactus_growth_modeling_qgam.R`.

367 Johnson's S_U and then the skewed t distributions, both of which are limited to positive
 368 excess kurtosis. Both distributions provided some improvement over the Gaussian, but
 369 were not happy with the fit of either. Iterating through the workflow (Fig. 1), we ar-
 370 rived, again, at the SHASH distribution, which is more flexible than either the JSU or
 371 skewed t , capable of capturing a greater range of kurtosis for a given amount of skew,
 372 and vice versa (Steve's NPSkewKurtosisRanges.pdf). Furthermore, fitting the SHASH
 373 as a generalized additive model with `mgcv` allowed for flexible, non-monotonic size-
 374 dependence in skewness and kurtosis without the need for model selection on specific
 375 size-dependent functions; through iterations of trial and error, we found this flexibility
 376 was necessary to generate simulated data that compared favorably to the real data. The
 377 other distributions that we tried are not available as `mgcv` families, so we fit these with
 378 custom maximum likelihood functions, an approach we illustrate in the next case study.
 379 The final growth model was similar to the SHASH gam in the coral case study, but
 380 with random intercepts for the location parameter, representing spatial and temporal
 381 heterogeneity:

```
382 fit_shash <- gam(list(logvol_t1 ~ s(logvol_t,k=4) +  

  383 s(plot,bs="re") + s(year_t,bs="re")), # <- model for locat
```

```

384 ~ s(logvol_t,k=4), # <- model for log-scale
385 ~ s(logvol_t,k=4), # <- model for skewness
386 ~ s(logvol_t,k=4)), # <- model for log-kurtosis
387 data = CYIM_grow,
388 family = shash,
389 optimizer = "efs")

```

390 The final SHASH model provided good correspondence between simulated and
391 real data, and provided more compelling improvement over the Gaussian model than
392 we saw in the coral case study (Fig. 7). The SHASH model over-estimated negative
393 skew at some sizes relative to the signal of skewness in the data (Fig. 7C), but the nature
394 of size-dependent skew in the data is not very biologically plausible and may instead
395 be driven by the tail-wagging tendency of gams. As in the coral case study, we see
396 that correctly modeling skewness and kurtosis improved estimation of the mean and
397 standard deviation (Fig. 7A,B), yielding a growth model that is clearly truer to the data
398 than the pilot Gaussian fit.

399 We explored how improved growth modeling influenced IPM results, leveraging
400 the plot and year structure of the study design to quantify spatial and temporal vari-
401 ance in fitness. We used the fitted random effects from the vital rate models to estimate
402 the asymptotic growth rate for each year (λ_t), centered on the average plot, and for
403 each plot (λ_p), centered on the average year. This allowed us to quantify demographic
404 variance associated with temporal and spatial heterogeneity. We found that the Gaus-
405 sian growth model tended to over-estimate λ_t , particularly in the harshest years (Fig.
406 8A), and thus under-estimated temporal variance in fitness ($Var(\lambda_{t(Gaussian)}) = 0.0018$,
407 $Var(\lambda_{t(SHASH)}) = 0.0023$). The opposite was true for plot-to-plot variation (Fig. 8B),
408 where the Gaussian model under-estimated λ_p and over-estimated spatial variance in
409 fitness ($Var(\lambda_{p(Gaussian)}) = 0.00015$, $Var(\lambda_{p(SHASH)}) = 0.000088$). Across both growth
410 models, fluctuations in fitness were stronger through time than across space. The
411 difference in temporal variance would suggest that Gaussian growth modeling would
412 lead to over-estimation of the stochastic growth rate λ_S , since temporal variance has
413 a negative influence on λ_S . However, this was not the case: stochastic IPMs based
414 on Gaussian and SHASH growth models had nearly identical stochastic growth rates
415 ($\lambda_S(Gaussian) = 0.9906$, $\lambda_S(Gaussian) = 0.9909$). This is likely because temporal fluctu-
416 ations in vital rates, which is where the SHASH growth model would make a difference,
417 have a weaker influence on λ_S than the temporal fluctuations in size structure that they
418 generate (Compagnoni et al., 2016; Ellis and Crone, 2013). Thus, depending on the target

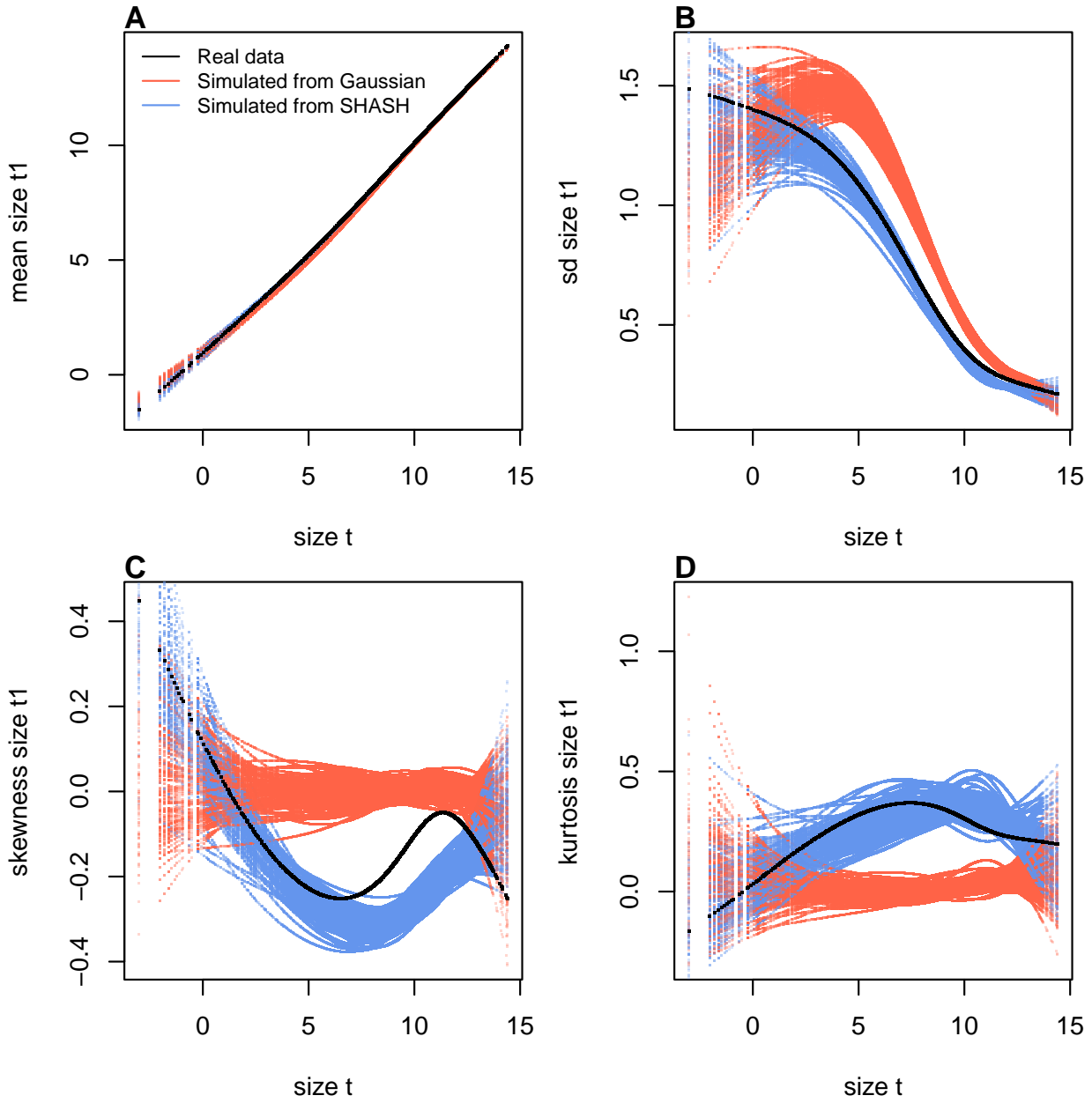


Figure 7: Comparisons among real cactus data and data simulated from Gaussian and SHASH growth models for mean, standard deviation, NP skewness, and NP kurtosis of future size conditional on current size. Figure made by script `cactus_growth_modeling_qgam.R`.

⁴¹⁹ of one's analysis, modeling non-Gaussian size transitions with a Gaussian growth model
⁴²⁰ could bias results in either direction, or make no difference at all.

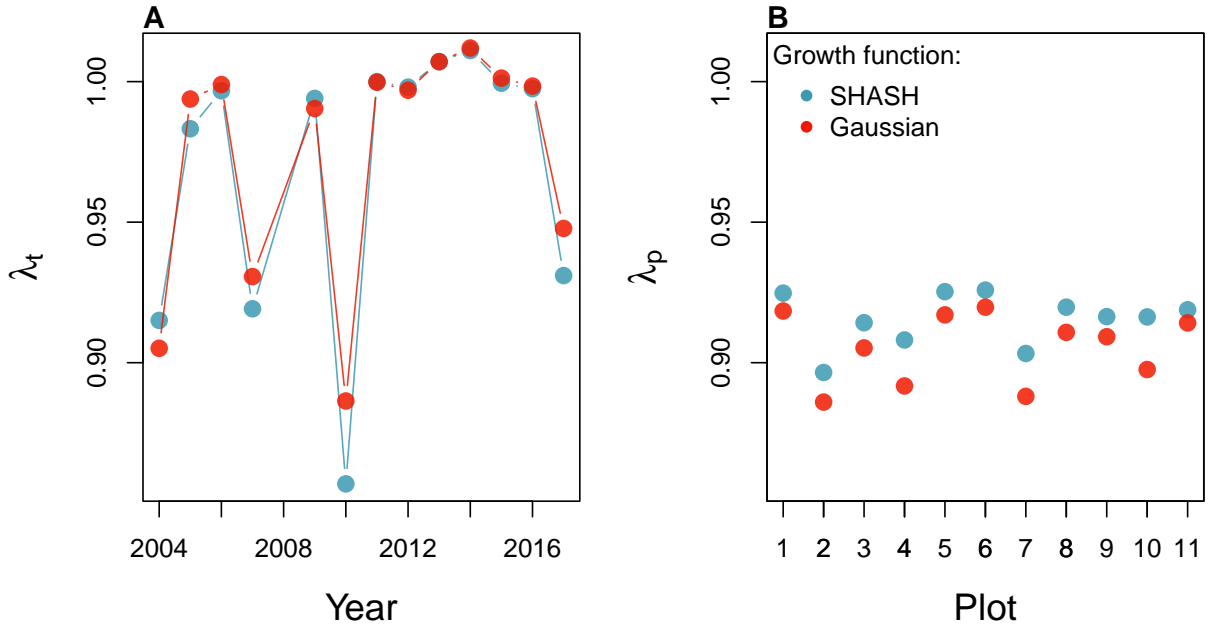


Figure 8: Temporal (A) and spatial (B) heterogeneity in fitness for the tree cholla cactus (*Cylindropuntia imbricata*) predicted by IPMs using Gaussian or SHASH growth models. Figure made by script `cactus_growth_modeling_qgam.R`.

421 3 Case study: creosotebush, *Larrea tridentata*

422 Our next case study comes from our studies of the woody shrub creosotebush (*Larrea tri-*
 423 *dentata*) at the Sevilleta Long-Term Ecological Research (LTER) site in central New Mex-
 424 ico, US. At this site as elsewhere in the Southwest US, creosotebush is encroaching into
 425 desert grassland habitats. The data described here were collected along transects span-
 426 ning grass-shrub ecotones to understand patterns of density dependence in creosotebush
 427 demography. Specifically, we asked whether fitness is maximized approaching zero den-
 428 sity at the leading edge of the expansion front (consistent with ‘pulled’ expansion), or
 429 whether there is a demographic advantage for shrubs at higher density due to positive
 430 feedbacks expected for ecosystem engineers (leading to ‘pushed’ expansion). Our pub-
 431 lished study (Drees et al., 2023) used a spatial integral projection model (SIPM) to predict
 432 the speed of shrub encroachment, assuming normally-distributed size transitions. Here
 433 we step through our suggested workflow to ask whether a non-Gaussian model would
 434 have been more faithful to the data, and how such an improvement would influence
 435 predictions for the speed of encroachment. We use this case study to illustrate several
 436 new elements and challenges, including modeling skewness and kurtosis as functions
 437 of expected future size (instead of initial size) and using distributions that are not cur-

438 recently available as **mgcv** families. In fact, to diversify our use of software and illustrate
439 alternatives, we do not use gam's for any element of this case study.

440 Growth data come from 522 shrubs censused longitudinally over four years (2013–
441 2017). Census individuals occurred along 12 replicate transects (200 to 600 m in length)
442 that spanned gradients of shrub density along shrub-grass ecotones. Size was measured
443 as volume of an elliptical cone based on height and width measurements; the size vari-
444 able of the IPM was the natural logarithm of volume (cm^3). For each census individual,
445 we recorded the size and density of all conspecifics within the five-meter transect “win-
446 dow” in which it occurred, and took the sum of all sizes within the window as a measure
447 of local density. The data are available in Ochocki et al. (2023).

448 As an initial Gaussian approach, we first fit a set of candidate generalized linear
449 mixed models, including transect as a random effect, that represented competing hy-
450 potheses for how size, density, and their interaction influence growth. Specifically, we fit
451 five candidate Gaussian models that included fixed effects of initial size only (model 1),
452 size and density (model 2), and size, density, and their interaction (model 3), allowing
453 for shrubs of different sizes to have different growth responses to local density. Models
454 4 and 5 mirrored models 2 and 3 but included second-order terms for density, allowing
455 for the possibility of non-monotonic density dependence. As in (Drees et al., 2023) we
456 pooled data across three transition years. Initial AIC rankings of these pilot models fa-
457 vor model 4 slightly over model 5 ($\Delta AIC = 0.8$) and significantly over all other models
458 ($\Delta AIC > 2$). However, these models were fit assuming constant variance, and inspection
459 of the residuals of the best model indicate this is not a safe assumption.

460 Unlike our previous case studies, here we have multiple fixed effects that may influ-
461 ence the variance of future size. In cases such as this, we recommend modeling variance
462 as a function of expected future size rather than initial size, as we did with the corals
463 and cacti. The expected (or “fitted”) values reflect the combined influence of all fixed
464 and random effects, and therefore implicitly account for multiple sources of variation in
465 the variance. While there are several convenient software packages for simultaneously
466 modeling Gaussian mean and variance as functions of independent variables (**mgcv** for
467 additive models as we saw above, **nlme** for linear models), **modeling variance as a func-**
468 tion of the mean is trickier because they cannot easily be fit simultaneously⁴. Here we
469 us an iterative re-weighting approach – which is not elegant, but it works. For Gaus-
470 sian models, weights w_i can be used to indicate that the observations y_i vary in their
471 dispersion around the mean. In general, the iterative steps are:

⁴After I wrote this I discovered that **nlme** can fit residual variance as a function of fitted(.)

1. Fit the expected value and normally-distributed residuals with constant variance:

$$y_i = \mu_i + \epsilon_i$$

$$\epsilon_i \sim N(0, \sigma)$$

2. Fit the standard deviation of the residuals as a function of the expected value.
Weights are derived as the inverse of the fitted variance:

$$\epsilon_i \sim N(0, f(\mu_i))$$

$$w_i = 1/f(\mu_i)^2$$

3. Re-fit the observation model, weighting the residual variance according to step 2:

$$y_i = \mu_i + \epsilon_i$$

$$\epsilon_i \sim N(0, \sigma \times \sqrt{w_i})$$

472 We iterated steps 2 and 3 until the weights did not change. In step 2, we modeled
473 the standard deviation as a simple linear function of the expected value ($\log(f(\mu_i)) =$
474 $\beta_0 + \beta_1 * \mu_i$) but other functions are possible, as is model selection among them. We
475 did this for all candidate models and, for fair AIC comparison, we re-fit all candidate
476 models with the same weights, estimated from the top model. The updated model
477 selection continued to favor model 4, but now with a stronger improvement over the
478 next-best model ($\Delta AIC = 3.0$).

479 The resulting Gaussian growth model predicts strong initial size-dependence and
480 weak and slightly nonlinear (but monotonic) negative density dependence (Fig. 9A).
481 The model accounts for non-constant variance through the fitted weights, which indicate
482 greater dispersion for smaller values of expected size ($\beta_1 = -0.21$; Fig. 9B). Quantiles of
483 the standardized residuals indicate weak negative skew (difference in tail size is 1–2%
484 of their total) and positive excess kurtosis, especially at smaller expected sizes (tails are
485 6–10% fatter than Gaussian) (Fig. 9C).⁵ As a candidate for improvement, we turned to
486 the Johnson's S_U (JSU) distribution, a four-parameter, leptokurtic distribution capable
487 of skew in either direction. We used a parameterization of the JSU for which location

5 Note that there is still a variance trend in the standardized residuals—rather unsatisfying! I have been through this backwards and forwards and my take is that this is a product of the sample size imbalance between small and large plants. The quantile regression is doing its best.

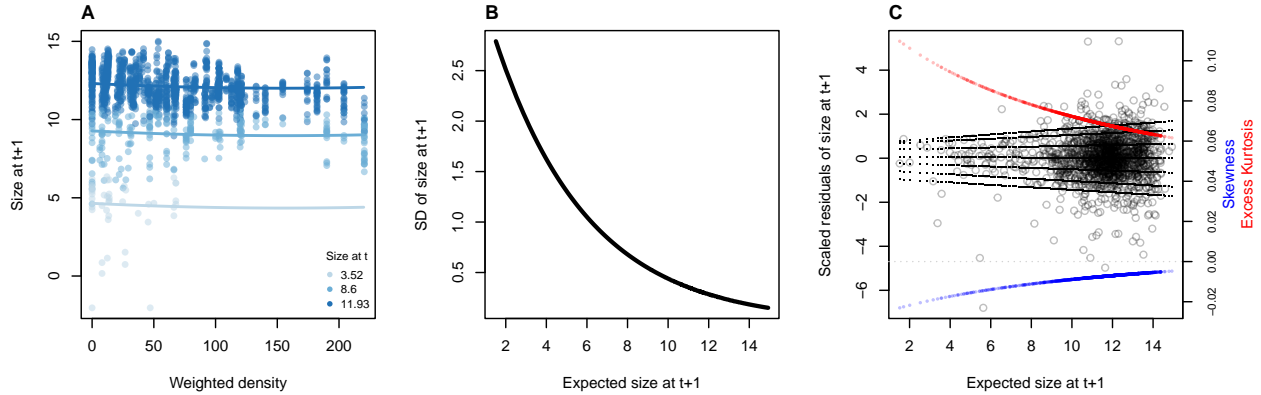


Figure 9: **A**, Creosotebush size transition data with respect to initial size (colors) and local weighted density (sum of sizes of all plants within a five-meter transect window). Size is quantified as the natural logarithm of plant volume (cm^3). **B**, Standard deviation of size at time $t + 1$ as a function of expected size at $t + 1$ (the fitted values), estimated by iterative re-weighting. **C**, Quantile regressions of scaled residuals on size and nonparametric estimates of skewness (blue) and excess kurtosis (red) derived from them. Black lines in **C** show the 5th, 10th, 25th, 50th, 75th, 90th, and 95th quantiles. Figure made by script `creosote_growth_modeling_qgam.R`.

488 parameter μ is the mean and scale parameter σ is the standard deviation (Rigby et al.,
 489 2019).

490 Like many of the non-Gaussian candidates that we suggest (Fig. 1), the JSU dis-
 491 tribution is not presently available as a family option for linear mixed models in any
 492 software package, to our knowledge. However, this need not be a barrier to using it for
 493 growth modeling. We fit a custom maximum likelihood model that borrows the mean
 494 and standard deviation of best Gaussian model and limits estimation of free parameters
 495 to those that control the JSU's skewness and kurtosis – effectively modeling the stan-
 496 dardized residuals rather than sizes. Here is what such a hybrid likelihood model looks
 497 like in practice:

```
498 ## log_volume_t1 are the size obervations
499 ## GAU_fitted are the expected values of the best Gaussian model
500 ## pars is a vector of free parameters to be estimated
501 JSULogLik=function(pars){
502   dJSU(x=log_volume_t1,
503   mu=GAU_fitted,
504   sigma=exp(GAU_sd_coef[1]+GAU_sd_coef[2]*GAU_fitted),
505   nu = pars[1]+pars[2]*GAU_fitted,
506   tau = exp(pars[3]+pars[4]*GAU_fitted), log=TRUE)
```

507 }

508 The mean of the JSU is set to that of the best Gaussian model (GAU_fitted) and the
509 standard deviation is a function of the mean according to the coefficients (GAU_sd_coef)
510 estimated through iterative re-weighting. Based on diagnostics of the standardized resid-
511 uals (Fig. 9), JSU parameters that control skewness and kurtosis are defined as linear
512 functions of the mean, and it is these coefficients that are estimated by maximum like-
513 lihood. Here we are relying on the robustness of Gaussian linear models to deviations
514 from normality . If one is skeptical of this approach, it is possible, as an alternative,
515 to simultaneously re-fit all parameters of the JSU in a maximum likelihood framework.
516 However, incorporating random effects into a custom likelihood model is non-trivial (we
517 provide guidance on one way to do this, using the “shrinkage” approach, in Appendix
518 XX). Therefore a key advantage of the hybrid approach is convenient retention of the
519 fitted random effects and associated variance components, which get shuttled from the
520 Gaussian model into the non-Gaussian model without any fuss (it was critical that we
521 used a parameterization of the JSU for which `mu` is the mean and `sigma` is the standard
522 deviation). And, if this approach does not “work” (i.e., deviations from normality bi-
523 ased the fitted values of the Gaussian model) one would quickly find out through the
524 simulation step of the workflow. In this case, the hybrid JSU model performed well,
525 generating simulated data that aligned with the real data better than the best Gaussian
526 model, particularly in **standard deviation**⁶ and kurtosis (Fig. 10). Note that in Fig. 10
527 we are plotting moments of the future size distribution with respect to initial size; this
528 distribution is also conditional on density but initial size is by far the stronger predictor
529 of future size, so we chose this visualization.

530 The improvement of the JSU over the Gaussian growth model, while visually satis-
531 fying, had virtually no influence on SIPM results. Models using Gaussian or JSU growth
532 kernels had nearly identical, monotonic decreases in λ with increasing local density, and
533 nearly identical wave velocities (Fig. 11). This species has very low mortality risk once
534 established (mean remaining life expectancy of a median-sized shrub is 24,408 years)
535 and its population growth and wave expansion are limited by very low seedling recruit-
536 ment ((Drees et al., 2023)). Weak size-dependence in survival likely explains why the
537 improvement in growth modeling had little influence on SIPM predictions.

⁶I am a little mystified as to why the JSU is so much better. It is literally the same SD in both distributions.

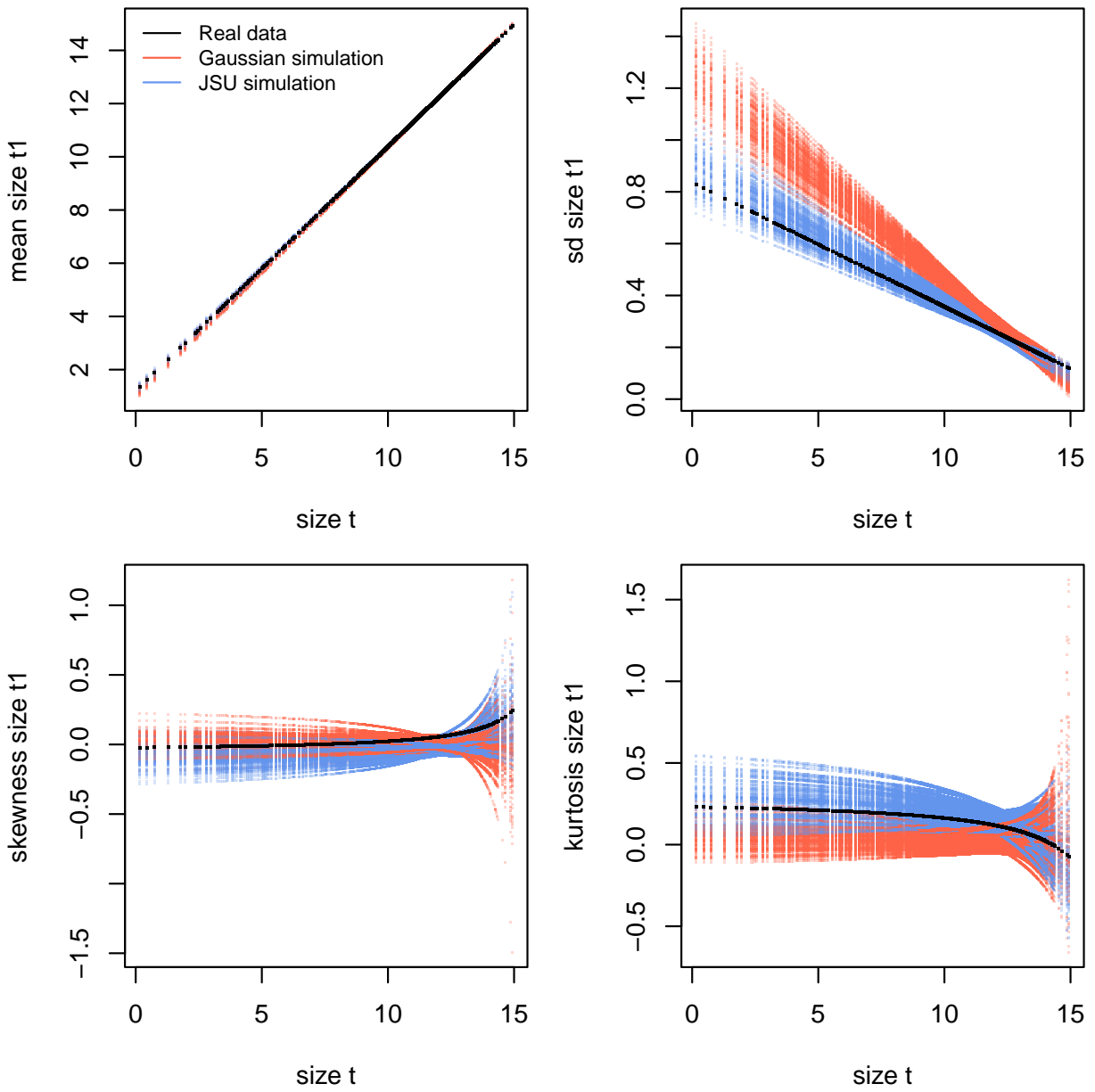


Figure 10: Comparisons between real creosotebush data and data simulated from Gaussian and JSU growth models for mean, standard deviation, NP skewness, and NP kurtosis of future size conditional on current size. Figure made by script `creosote_growth_modeling_qgam.R`.

538 4 Case study: lady orchid, *Orchis purpurea*

539 Our final case study examines selection on life history strategies in the lady orchid *Or-*
 540 *chis purpurea*. In a prior study, Miller et al. 2012 contrasted the growth trajectories from
 541 year t to $t + 1$ for plants that did or did not flower in year t , as a way to quantify costs

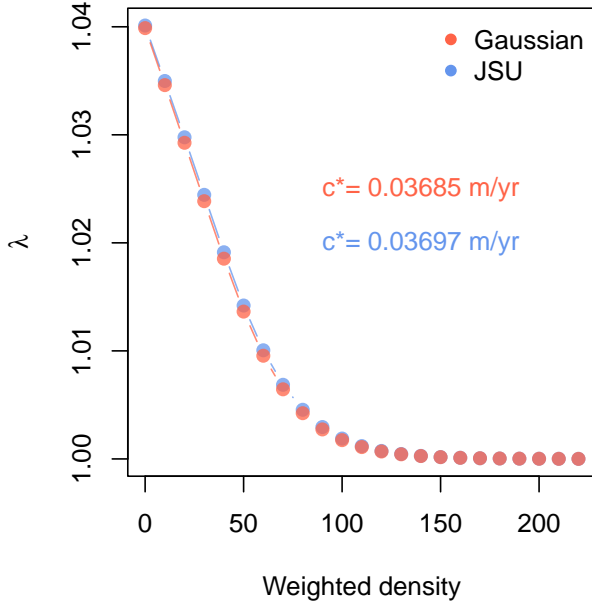


Figure 11: Density dependence in fitness (λ) and asymptotic velocity of the creosote encroachment wave (c^*) for Gaussian and JSU growth kernels. Weighted density is the sum of sizes ($\log(cm^3)$) of all conspecifics within a five-meter transect “window”. Figure made by script `creosote_growth_modeling_qgam.R`.

of reproduction. The different growth kernels were then used in an IPM to quantify evolutionarily stable life history strategies: the optimal flowering size that balances benefits of flowering at larger sizes against the risk of dying before reaching those sizes. The original study assumed a Gaussian distribution of size transitions and allowed for non-constant variance with respect to initial size. Here we re-visit that analysis applying our growth modeling workflow to derive improved growth kernels for flowering and non-flowering orchids.

The data, originated by Dr. Hans Jacquemyn and used here with permission, come from 368 plants in a Belgian population that was censused annually from 2003 through 2011 (for this reanalysis we are using data only from the “light” habitat). Size was measured as leaf area (cm^3) summed over all leaves, and we analyzed the natural logarithm of total leaf area as the size variable of the IPM.

As a pilot Gaussian approach, we fit six candidate models in which the mean was a function of initial size only, additive effects of initial size and flowering status, and interaction between size and flowering, and the standard deviation was a function of size only (models 1-3) or size and flowering status (models 4-6). All models included a random intercept for year. As another variation on software and an alternative to two-

559 step fitting or iterative re-weighting, here we use `nmle::lme()`, which can simultaneously
560 fit linear predictors for mean and variance. For example, model 1 was:

```
561 orchid_GAU[[1]]<-lme(log_area_t1~ log_area_t,  
562 weights=varExp(form=~ log_area_t),  
563 random=~ 1|begin.year,data=orchid_grow,method="ML")
```

564 Model 3 (size \times flowering) was strongly favored, consistent with prior results that non-
565 flowering plants have a growth advantage over flowering plants. Growth variance de-
566 clined with initial size for both reproductive classes (Fig. 12A-B) and skewness and kur-
567 tosis of the standardized residuals indicate strong deviations from normality (Fig. 12C-
568 D). For most sizes, left skew and excess kurtosis were more severe for non-reproductive
569 plants, with tail imbalance ca. 10% of their total and tail weights 10–20% fatter than
570 Gaussian.

571 As improvements, we explored the skewed *t* and Johnson's SU distributions, both
572 leptokurtic distributions with flexible skewness. We were happier with the skewed *t*,
573 which we fit in a similar way as we fit the JSU to the creosote data, setting the mean
574 and standard deviation to the Gaussian fits and estimating free parameters controlling
575 skewness and kurtosis:

```
576 ## log_area_t1 and log_area_t are the size obervations  
577 ## flowering indicates reproductive status at time t (0 or 1)  
578 ## GAU_fitted and GAU_sd are mean and standard deviation from lme  
579 ## pars is a vector of free parameters to be estimated  
580 SSTLogLik=function(pars){  
581     dSST(x=log_area_t1,  
582             mu=GAU_fitted,  
583             sigma=GAU_sd,  
584             nu = exp(pars[1] + pars[2]*log_area_t + pars[3]*as.logical(flowering) + pars[4])  
585             tau = exp(pars[5] + pars[6]*log_area_t + pars[7]*as.logical(flowering) + pars[8])  
586             log=TRUE)  
587 }
```

588 `gamlss.dist:dSST` is a parameterization of the skewed *t* in which `mu` and `sigma` are the
589 mean and standard deviation, respectively. Based on diagnostics of the standardized
590 residuals (Fig. 12) we allowed `nu` and `tau` to vary by size and differ between flowering
591 and non-flowering plants (note that the `tau` parameter uses a $\log(x - 2)$ link function).
592 Size transition data simulated from this model corresponded favorably to the real data,

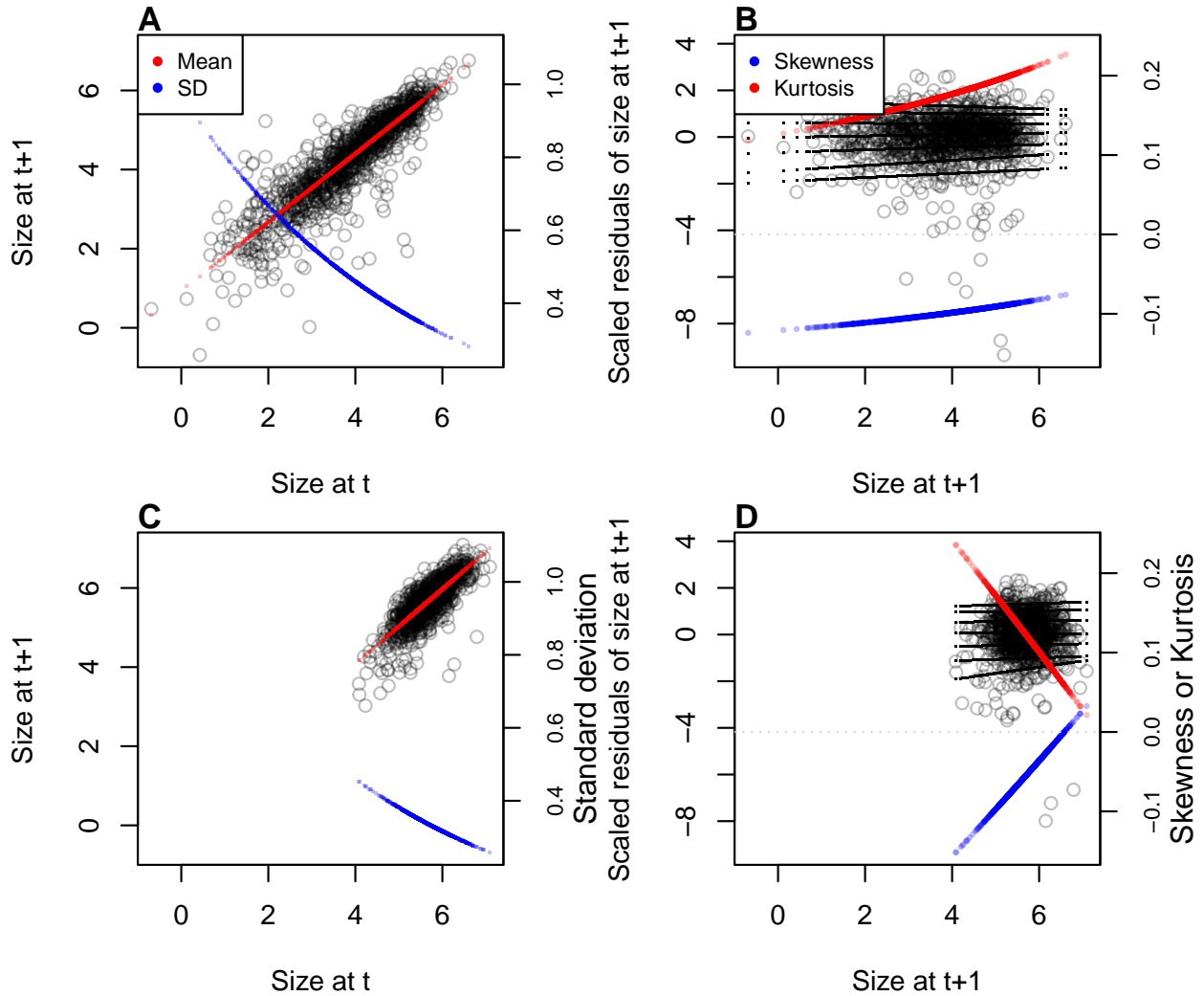


Figure 12:

593 much better than the pilot Gaussian model, including improvements in the **standard**
 594 **deviation**⁷, skewness, and kurtosis of future size (Fig. 13).

595 Finally, we used the improved growth model to revisit key results of the original
 596 study. Miller et al. (2012) used the orchid IPM to estimate the evolutionarily stable strat-
 597 egy (ESS) as the mean size at flowering that maximizes lifetime reproductive success
 598 (R_0), given the constraint that flowering when small reduces growth and thus elevates
 599 mortality risk. Repeating that analysis here, we found that improved growth modeling
 600 has virtually no influence on predictions for optimal life history strategies (Fig. 14). ESS
 601 flowering sizes were nearly identical between IPMs with Gaussian vs skewed t growth
 602 models, and both aligned well with the observed mean flowering size (dashed vertical

⁷Again, the improvement here is surprising to me and I am unsure what to say about it.

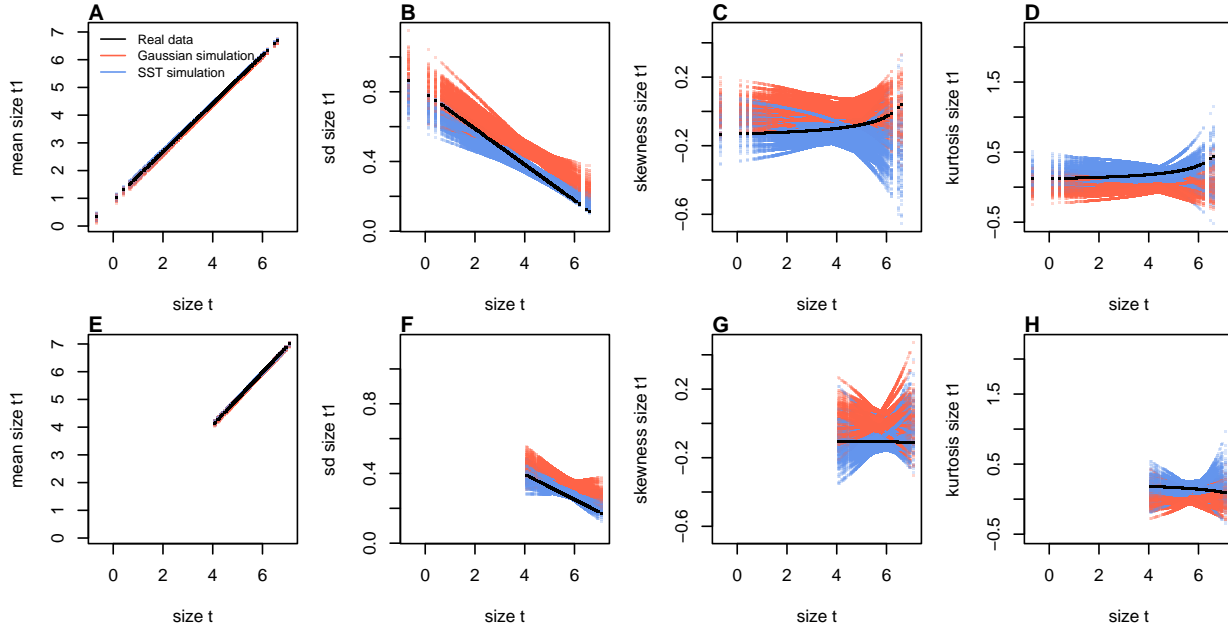


Figure 13: Comparisons between real orchid data and data simulated from Gaussian and skewed t growth models for mean, standard deviation, NP skewness, and NP kurtosis of future size conditional on current size. Top row (A-D) shows plants that were vegetative at the start of the transition year and bottom row (E-H) shows plants that were flowering at the start of the transition year. Figure made by script `orchid_growth_modeling_rq.R`.

line in Fig. 14A). Extending beyond the original study, we also explored expected remaining lifespan for different ages and sizes (R package **Rage** (Jones et al., 2022)). Gaussian and skewed t growth models predicted nearly identical mean remaining lifespans across the stage and size distribution (Fig. 14B). However, the skewed t model predicted consistently greater variance in remaining lifespan, nearly 10% greater at some sizes.⁸ Thus, as we have seen in other case studies, the practical consequences of improved growth modeling depend on what one aims to learn from the IPM.

5 Discussion

Much of the appeal of integral projection models has stemmed from their embrace of continuous size structure through reliance on regression-based approaches, and the potentially complex fixed- and random-effect structures that these approaches allow. Using familiar statistical tools and with relatively few parameters to estimate, IPM users can

⁸Do not believe this result! I have left it here as a placeholder because I would like to do this correctly. But I think there are problems with `Rage's life_expect_var()` function. The predicted variance declines linearly with matrix dimension.

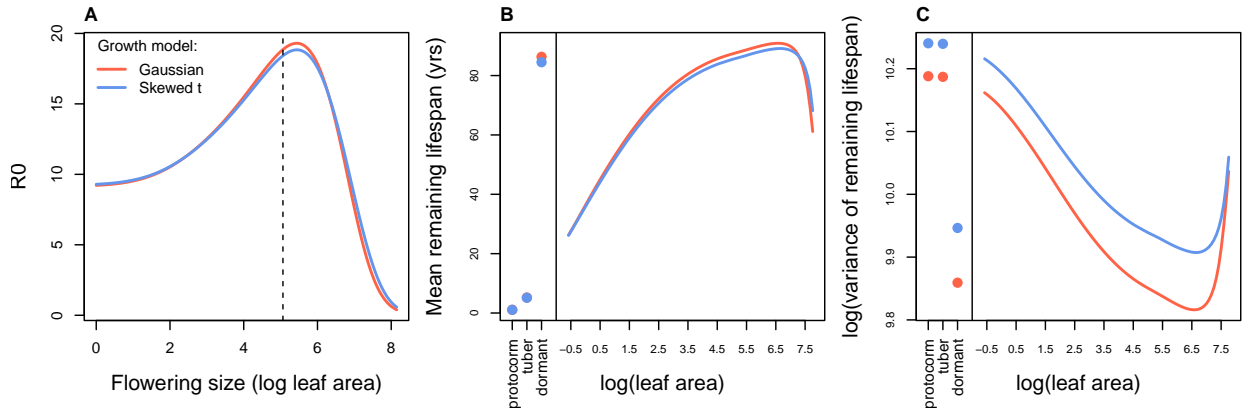


Figure 14: Orchid life history results from IPMs using Gaussian or skewed t growth models. **A**, Lifetime reproductive success (R_0) as a function of mean size of flowering. Dashed vertical line shows the observed mean flowering size. **B-C**, Mean and variance of remaining lifespan as a function of size or stage. The orchid IPM includes three discrete below-ground stages (protocorm, tuber, and dormant plant) in addition to continuous size of above-ground plants.

incorporate important sources of variation in demography and interrogate their influence on ecological and evolutionary dynamics. With this opportunity comes the extra burden of getting it right: IPMs are good models of the populations they are intended represent only insofar as the statistical models provide good fits to the underlying data. The growth sub-model is the trickiest part of “getting it right” because it defines a distribution of future size conditional on current size. Distributions have many properties – “moments” – and a good growth model should recapitulate the properties of real size transitions. The default assumption of normally distributed size transitions, employed overwhelmingly across 20+ years of IPM studies, is an arbitrary historical precedent. In four case studies (chosen simply because we had the data at our fingertips) and, we suspect, more broadly, skewness and excess kurtosis were common features of size transition data: shrinking was more common than growing, and large changes in size were more common than a Gaussian model would predict. Our most important message is that the standard assumption of normally-distributed size transitions should be abandoned and a more inquisitive process of growth modeling should take its place.

We have attempted to lay out a general workflow for what that process should look like, guided by visual diagnostics of standardized residuals. One implication of relying on visual diagnostics is that goodness of fit is in the eye of the beholder. This approach can empower IPM users to make informed choices, but it is not very prescriptive: we have not suggested any hard rules for when one or another distribution should be used.

635 Alternatively, model selection could be used to identify best-fitting growth distributions
636 and best-fitting functions for higher moments. However, model selection among growth
637 distributions with 3-5 parameters, each of which may be functions of state variables or
638 fitted values, can quickly explode in complexity. A good growth model should generate
639 data that look like the real thing, and it should be possible to find a good one without
640 worrying about which one is objectively “best”.

641 In all of our case studies, non-Gaussian growth models always yielded more sat-
642 isfying fits to size transition data than the Gaussian models published in those papers.
643 However, much to our relief, none of these re-analyses yielded a “gotcha” result that
644 overturned results of the original study. In this small sampling of case studies, im-
645 proved growth modeling had only modest effects on IPM results. We caution against
646 taking too much comfort in this outcome; we can imagine other scenarios in which the
647 choice of the growth distribution could be more consequential. It is worth noting that
648 three of our case studies focused on perennial plants and the fourth focused on corals,
649 which are demographically similar to perennial plants (heavy losses during recruitment
650 but high survival once established). Life cycles such as these may be relatively robust to
651 subtle features of the growth kernel. More systematic comparative analyses across may
652 provide insight into which types of species and life histories are more likely to exhibit
653 strong skewness and kurtosis of size transitions, and the conditions under which demo-
654 graphic analysis is more or less sensitive to these features of size transition. It is also
655 worth noting, as we saw in several case studies, that different outputs from the same
656 model can be more or less sensitive to the choice of growth distribution.

657 Some issues to be discussed.

- 658 • Many software options: lme4/maxLik, mgcv, rstan
- 659 • Comparison of our approach with beta regression method.
- 660 • We have emphasize growth but same principles apply to other continuous state
661 transitions, eg disease IPMs.
- 662 • Same issues apply to MPMs

663 Acknowledgements

664 This research was supported by US NSF grants DEB-1933497 to SPE and DEB-1754468,
665 2208857, and 2225027 to TEXM.

666 6 Authorship statement

667 All authors discussed all aspects of the research and contributed to developing methods,
668 analyzing data, and writing and revising the paper.

669 7 Data accessibility statement

670 No original data appear in this paper. Should the paper be accepted, all computer scripts
671 supporting the results will be archived in a Zenodo package, with the DOI included at
672 the end of the article. During peer review, our data and code are available at https://github.com/texmiller/IPM_size_transitions.
673

674 Literature Cited

- 675 Anscombe, F. J. and Glynn, W. J. (1983). Distribution of the kurtosis statistic b_2 for
676 normal samples. *Biometrika*, 70(1):227–234.
- 677 Bates, D., Sarkar, D., Bates, M. D., and Matrix, L. (2007). The lme4 package. *R package
678 version*, 2(1):74.
- 679 Bruno, J. F., Ellner, S. P., Vu, I., Kim, K., and Harvell, C. D. (2011). Impacts of aspergillosis
680 on sea fan coral demography: modeling a moving target. *Ecological Monographs*,
681 81(1):123–139.
- 682 Compagnoni, A., Bibian, A. J., Ochocki, B. M., Rogers, H. S., Schultz, E. L., Sneck, M. E.,
683 Elderd, B. D., Iler, A. M., Inouye, D. W., Jacquemyn, H., et al. (2016). The effect of
684 demographic correlations on the stochastic population dynamics of perennial plants.
685 *Ecological Monographs*, 86(4):480–494.
- 686 Conn, P. B., Johnson, D. S., Williams, P. J., Melin, S. R., and Hooten, M. B. (2018). A guide
687 to bayesian model checking for ecologists. *Ecological Monographs*, 88(4):526–542.
- 688 Cooch, E. G. and White, G. C. (2020, accessed 5/17/2020). *Program MARK - a 'gentle
689 introduction'*. Available at phidot.org.
- 690 Coulson, T. (2012). Integral projections models, their construction and use in posing
691 hypotheses in ecology. *Oikos*, 121(9):1337–1350.
- 692 Crone, E. E. (2016). Contrasting effects of spatial heterogeneity and environmental
693 stochasticity on population dynamics of a perennial wildflower. *Journal of Ecology*,
694 104(2):281–291.
- 695 Czachura, K. and Miller, T. E. (2020). Demographic back-casting reveals that subtle
696 dimensions of climate change have strong effects on population viability. *Journal of
697 Ecology*.
- 698 D'Agostino, R. B. (1970). Transformation to normality of the null distribution of g_1 .
699 *Biometrika*, pages 679–681.
- 700 Davis, C. (2015). *sgt: Skewed Generalized T Distribution Tree*. R package version 2.0.
- 701 Drees, T., Ochocki, B. M., Collins, S. L., and Miller, T. E. (2023). Demography and
702 dispersal at a grass-shrub ecotone: a spatial integral projection model for woody plant
703 encroachment. *Ecological Monographs*, page e1574.

- 704 Easterling, M. R., Ellner, S. P., and Dixon, P. M. (2000). Size-specific sensitivity: applying
705 a new structured population model. *Ecology*, 81(3):694–708.
- 706 Elderd, B. D. and Miller, T. E. (2016). Quantifying demographic uncertainty: Bayesian
707 methods for integral projection models. *Ecological Monographs*, 86(1):125–144.
- 708 Ellis, M. M. and Crone, E. E. (2013). The role of transient dynamics in stochastic popula-
709 tion growth for nine perennial plants. *Ecology*, 94(8):1681–1686.
- 710 Ellner, S. P., Adler, P. B., Childs, D. Z., Hooker, G., Miller, T. E., and Rees, M. (2022).
711 A critical comparison of integral projection and matrix projection models for demo-
712 graphic analysis: Comment. *Ecology*, 103(10):e3605.
- 713 Ellner, S. P., Childs, D. Z., and Rees, M. (2016). *Data-driven Modeling of Structured Popula-*
714 *tions: A Practical Guide to the Integral Projection Model*. Springer, New York.
- 715 Gould, W. R. and Nichols, J. D. (1998). Estimation of temporal variability of survival in
716 animal populations. *Ecology*, 79:2531 – 2538.
- 717 Gu, C. (2013). *Smoothing Spline ANOVA Models*. Springer Science+Business Media, New
718 York, 2 edition.
- 719 Hadfield, J. D. et al. (2010). Mcmc methods for multi-response generalized linear mixed
720 models: the mcmcglmm r package. *Journal of Statistical Software*, 33(2):1–22.
- 721 Héault, B., Bachelot, B., Poorter, L., Rossi, V., Bongers, F., Chave, J., Paine, C. T., Wagner,
722 F., and Baraloto, C. (2011). Functional traits shape ontogenetic growth trajectories of
723 rain forest tree species. *Journal of ecology*, 99(6):1431–1440.
- 724 Jones, M. and Pewsey, A. (2009). *Biometrika*, 96:761 – 780.
- 725 Jones, M. C., Rosco, J. F., and Pewsey, A. (2011). Skewness-invariant measures of kurtosis.
726 *The American Statistician*, 65(2):89 – 95.
- 727 Jones, O. R., Barks, P., Stott, I., James, T. D., Levin, S., Petry, W. K., Capdevila, P., Che-
728 Castaldo, J., Jackson, J., Römer, G., et al. (2022). Rcompadre and rage—two r pack-
729 ages to facilitate the use of the compadre and comadre databases and calculation of
730 life-history traits from matrix population models. *Methods in Ecology and Evolution*,
731 13(4):770–781.
- 732 Komsta, L. and Novomestky, F. (2015). Moments, cumulants, skewness, kurtosis and
733 related tests. *R package version*, 14(1).

- ⁷³⁴ Link, W. A. and Nichols, J. D. (1994). On the importance of sampling variance to investigations of temporal variation in animal population size. *Oikos*, 69(3):539 – 544.
- ⁷³⁵
- ⁷³⁶ Louthan, A. M., Keighron, M., Kiekebusch, E., Cayton, H., Terando, A., and Morris, W. F. (2022). Climate change weakens the impact of disturbance interval on the growth rate of natural populations of venus flytrap. *Ecological Monographs*, 92(4):e1528.
- ⁷³⁷
- ⁷³⁸
- ⁷³⁹ McGillivray, H. (1986). Skewness and asymmetry: measures and orderings. *Annals of Statistics*, 14:994–1011.
- ⁷⁴⁰
- ⁷⁴¹ Metcalf, C. J. E., Ellner, S. P., Childs, D. Z., Salguero-Gómez, R., Merow, C., McMahon, S. M., Jongejans, E., and Rees, M. (2015). Statistical modelling of annual variation for inference on stochastic population dynamics using Integral Projection Models. *Methods in Ecology and Evolution*, 6:1007–1017.
- ⁷⁴²
- ⁷⁴³
- ⁷⁴⁴
- ⁷⁴⁵ Miller, T. E. (2020). Long-term study of tree cholla demography in the los pinos mountains, sevilleta national wildlife refuge. <https://doi.org/10.6073/pasta/dd06df3f950afe4a4642306182237d13>.
- ⁷⁴⁶
- ⁷⁴⁷
- ⁷⁴⁸ Miller, T. E., Louda, S. M., Rose, K. A., and Eckberg, J. O. (2009). Impacts of insect herbivory on cactus population dynamics: experimental demography across an environmental gradient. *Ecological Monographs*, 79(1):155–172.
- ⁷⁴⁹
- ⁷⁵⁰
- ⁷⁵¹ Miller, T. E., Williams, J. L., Jongejans, E., Brys, R., and Jacquemyn, H. (2012). Evolutionary demography of iteroparous plants: incorporating non-lethal costs of reproduction into integral projection models. *Proceedings of the Royal Society B: Biological Sciences*, 279(1739):2831–2840.
- ⁷⁵²
- ⁷⁵³
- ⁷⁵⁴
- ⁷⁵⁵ Ochocki, B. M., Drees, T., and Miller, T. E. (2023). Density-dependent demography of creosote bush (*larrea tridentata*) along grass-shrub ecotones. <https://doi.org/10.6073/pasta/ca53c16f16dcf9fb11f3ee99ea5445ac>.
- ⁷⁵⁶
- ⁷⁵⁷
- ⁷⁵⁸ Ohm, J. R. and Miller, T. E. (2014). Balancing anti-herbivore benefits and anti-pollinator costs of defensive mutualists. *Ecology*, 95(10):2924–2935.
- ⁷⁵⁹
- ⁷⁶⁰ Ozgul, A., Childs, D. Z., Oli, M. K., Armitage, K. B., Blumstein, D. T., Olson, L. E., Tuljapurkar, S., and Coulson, T. (2010). Coupled dynamics of body mass and population growth in response to environmental change. *Nature*, 466(7305):482–485.
- ⁷⁶¹
- ⁷⁶²

- 763 Peterson, M. L., Morris, W., Linares, C., and Doak, D. (2019). Improving structured
764 population models with more realistic representations of non-normal growth. *Methods*
765 in Ecology and Evolution, 10(9):1431–1444.
- 766 Plard, F., Schindler, S., Arlettaz, R., and Schaub, M. (2018). Sex-specific heterogeneity
767 in fixed morphological traits influences individual fitness in a monogamous bird
768 population. *The American Naturalist*, 191(1):106–119.
- 769 Rees, M., Childs, D. Z., and Ellner, S. P. (2014). Building integral projection models: a
770 user's guide. *Journal of Animal Ecology*, 83(3):528–545.
- 771 Rigby, R. A., Stasinopoulos, M. D., Heller, G. Z., and De Bastiani, F. (2019). *Distributions*
772 for modeling location, scale, and shape: Using GAMLSS in R. CRC press.
- 773 Salguero-Gómez, R. and Casper, B. B. (2010). Keeping plant shrinkage in the demo-
774 graphic loop. *Journal of Ecology*, 98(2):312–323.
- 775 Schielzeth, H., Dingemanse, N. J., Nakagawa, S., Westneat, D. F., Allegue, H., Teplitsky,
776 C., Réale, D., Dochtermann, N. A., Garamszegi, L. Z., and Araya-Ajoy, Y. G. (2020).
777 Robustness of linear mixed-effects models to violations of distributional assumptions.
778 *Methods in ecology and evolution*, 11(9):1141–1152.
- 779 Schultz, E. L., Eckberg, J. O., Berg, S. S., Louda, S. M., and Miller, T. E. (2017). Native
780 insect herbivory overwhelms context dependence to limit complex invasion dynamics
781 of exotic weeds. *Ecology letters*, 20(11):1374–1384.
- 782 Stasinopoulos, D. M., Rigby, R. A., et al. (2007). Generalized additive models for location
783 scale and shape (gamlss) in r. *Journal of Statistical Software*, 23(7):1–46.
- 784 Stubberud, M. W., Vindenes, Y., Vøllestad, L. A., Winfield, I. J., Stenseth, N. C., and Lan-
785 gangen, Ø. (2019). Effects of size-and sex-selective harvesting: An integral projection
786 model approach. *Ecology and Evolution*, 9(22):12556–12570.
- 787 Wan, X., Wang, W., Liu, J., and Tong, T. (2014). Estimating the sample mean and stan-
788 dard deviation from the sample size, median, range and/or interquartile range. *BMC*
789 *medical research methodology*, 14:1–13.
- 790 Williams, J. L., Miller, T. E., and Ellner, S. P. (2012). Avoiding unintentional eviction from
791 integral projection models. *Ecology*, 93(9):2008–2014.

⁷⁹² Wood, S. (2017). *Generalized Additive Models: An Introduction with R.* Chapman and
⁷⁹³ Hall/CRC, 2 edition.

⁷⁹⁴ Zhang, J. L. (2014). Comparative investigation of three bayesian p values. *Computational
795 Statistics & Data Analysis*, 79:277–291.

Appendices

796 S.1 The Jones-Pewsey distribution

797 Jones and Pewsey (2009) introduced a simple, tractable generalization of the Normal dis-
798 tribution with two additional parameters determining asymmetry (skewness), and tail
799 weight (kurtosis) which can be either lighter or heavier than the Gaussian. It is defined
800 as a transformation of a $\text{Normal}(0,1)$ random variable using the hyperbolic sine func-
801 tion (\sinh) and its inverse (asinh), as follows. The distribution family's base probability
802 density $f_{\epsilon,\delta}$ is the probability density of the random variable $X_{\epsilon,\delta}$ where

$$803 \quad Z = \sinh(\delta \text{ asinh}(X_{\epsilon,\delta}) - \epsilon) \quad (\text{S.1})$$

804 and Z has a $\text{Normal}(0,1)$ distribution. Equivalently,

$$805 \quad X_{\epsilon,\delta} = \sinh\left(\frac{1}{\delta} \text{ asinh}(Z) + \frac{\epsilon}{\delta}\right). \quad (\text{S.2})$$

806 Parameters $\delta = 1, \epsilon = 0$ give the $\text{Normal}(0,1)$ distribution. Skewness has the sign of ϵ ,
807 and $\delta > 0$ controls tail weight, with heavier than Gaussian tails for $\delta < 1$ and lighter
808 than Gaussian tails for $\delta > 1$. A formula for the density $f_{\epsilon,\delta}$ is given by Jones and Pewsey
809 (2009, eqn. 2). The general four-parameter family with location parameter μ and scale
810 parameter σ is defined as the probability densities of $\mu + \sigma X_{\epsilon,\delta}$. We refer to this as the
811 JP distribution family.

812 As is unfortunately the case for most four-parameter distributions μ is not the mean,
813 σ is not the standard deviation, ϵ is not the skew and δ is not the kurtosis. All else being
814 equal, larger μ gives a larger mean, larger σ gives a higher standard deviation, higher
815 ϵ gives higher asymmetry, and higher δ gives heavier tail weight. But each moment is
816 jointly determined by all four parameters.

817 The main advantage of the JP distribution is that the attainable combinations of
818 skewness and kurtosis are very broad, compared to other four-parameter families, and
819 come very close to the theoretical limits on kurtosis as a function of skewness (Jones and
820 Pewsey, 2009, Fig. 2). Additionally, being a transformation of the Normal makes it very
821 simple to generate random numbers from the distribution, and to compute probability
822 density, cumulative distribution, and quantile functions. There are also simple analytic
823 formulas for the first four moments (Jones and Pewsey, 2009, p. 764) which we use below

824 to define a centered and scaled version in which μ and σ are the mean and standard
825 deviation.

826 The definition (S.2) shows that the distribution depends on ϵ only through the ratio
827 ϵ/δ . We have found that this property can be problematic for estimating distribution
828 parameters. Even with good sized ($n = 250$ or 500) data sets generated from the distri-
829 bution with known parameters, both maximum likelihood and Bayesian estimation were
830 unstable for some values of ϵ and δ , occasionally yielding estimates far from the truth.
831 One cause was a ridge in the (ϵ, δ) likelihood surface with a constant of ϵ/δ . Another is
832 that when δ is large, changes in ϵ have little effect.

833 To avoid that problems, we reparameterize the distribution as follows:

834
$$X_{\lambda, \tau} = \sinh(e^{-\tau} \operatorname{asinh}(Z) + \lambda). \quad (\text{S.3})$$

835 Thus, the two parameterizations are related by

836
$$\delta = e^\tau, \epsilon = \delta\lambda = e^\tau\lambda. \quad (\text{S.4})$$

837 The definition of τ allows it to take any real value, with negative values giving thinner
838 than Gaussian tails and positive values giving fatter than Gaussian tails. λ also can take
839 any real value, and the distribution's skew has the same sign as λ . Because the sinh
840 function is nonlinear, it is still the case that the skew depends on τ as well as λ , but the
841 "crosstalk" between the kurtosis and skew parameters is weaker. As a result, we found
842 that maximum likelihood estimation of parameter values was generally more reliable if
843 the distribution is parameterized in terms of τ and λ .

844 S.2 Estimating mixed-effects models using shrinkage

845 Ecologists often fit demographic and other statistical models that include random effects
846 terms to quantify variation among years, spatial locations, individuals, etc. Random
847 effects are a natural choice when interest centers on the magnitude of variation (e.g., how
848 much does mortality vary among years?) rather than individual values (e.g., mortality
849 in 2013). They also allow each estimate to "borrows strength" from others, so that (for
850 example) the estimate from a year with small sample size (and thus large sampling
851 variability) is shifted towards the center of the overall distribution.

852 Specialized software is often used to fit such models, such as the **nlme**, **lme4**, **mgee**
853 and **gamm4** libraries in R, but these only allow a small subset of the distribution families

854 we want to consider for modeling growth increments (the **gamlss** package allows many
855 distribution families, but in our experience, even when random effects are simple in
856 structure the fitting algorithms often fail to converge or fail to find the global optimum).

857 One way past this limitation is Bayesian estimation, using STAN with user-written
858 (or borrowed) code for the chosen growth distribution (see section XX for an example).
859 In this appendix we describe another option, introduced by Link and Nichols (1994)
860 and Gould and Nichols (1998): fitting a fixed-effects model by Maximum Likelihood,
861 followed by shrinkage of coefficient estimates. None of the ideas here are original. The
862 material overlaps Appendix S1 of Metcalf et al. (2015), but for completeness we make
863 it self-contained. Appendix D of Cooch and White (2020) (written by K.D. Burnham)
864 provides more details and examples in the context of capture-recapture analysis.

865 Here we explain shrinkage using a simple model based on our analysis of *Pseu-*
866 *doroegneria spicata*. That model includes random effects for between-year variation in
867 the slope and intercept of future size (log area) as a function of initial size. To keep
868 the example simple, we assume that initial size and year are the only covariates, and
869 we assume that growth increments follow a skew-Normal distribution with noncon-
870 stant variance and constant skew parameter. Code for this example is in the script
871 `SimpleShrinkageExample.R`. The first part of the script generates an artificial data set
872 by fitting the model to a subset of the growth data (20th century Control plots), and
873 randomly generating new “size next year” values for each individual in the actual data
874 set. The second part contains the “data” analysis.

875 As in our *P. spicata* analysis, we assumed that that the skew and kurtosis parameters
876 were functions of the location parameter; this dominated ($\Delta AIC \approx 30$) the alternate
877 model with skew and kurtosis depending on initial size. The analogous Gaussian model,
878 with constant variance, could be fitted as follows using `lmer`:

879 `lmer(new.size ~ init.size + (init.size|year), data=growthData, REML=TRUE);`
880 where `growthData` is a data frame holding the data with `year` as an unordered factor.
881 For our skew-Normal model, we instead use maximum likelihood with all between-year
882 variation included as fixed effects. The appropriate design matrix is easily constructed
883 using the `model.matrix` function:

884 `U = model.matrix(~ year + init.size:year - 1, data=growthData)`

885 If there are T years, the matrix `U` specified in this way has $2T$ columns corresponding to
886 n annual intercepts and T annual slopes.

Using this design matrix, we can readily write a log likelihood function for use with the **maxLik** package, with a log link function for the variance because it is necessarily positive:

```

890 LogLik=function(pars,new.size,U){
891   pars1 = pars[1:ncol(U)]; pars2=pars[-(1:ncol(U))];
892   mu = U%*%pars1;
893   sigma = exp(pars2[1]+pars2[2]*mu);
894   dSN1(new.size, mu=mu, sigma=sigma, nu=pars2[3], log=TRUE)
895 }
```

Parameters and their standard errors can then be estimated with **maxLik**, starting from a random guess:

```

898 start=c(runif(ncol(U)), rep(0,3))
899 out=maxLik(logLik=LogLik,start=start, new.size=simData$new.size,U=U,
900   method="BHHH",control=list(iterlim=5000,printLevel=1),finalHessian=TRUE);
901 coefs = out$estimate; # parameters
902 V = vcov(out); SEs = sqrt(diag(V)); # standard errors
```

In real life we would repeat the optimization several times with several different starting values, to be confident that the optimal parameter values had been found.

Focus now on the year-specific intercept parameters $\hat{a}_t, t = 1, 2, \dots, T$. We can view the year-specific estimates \hat{a}_t as consisting of unobserved true values a_t plus sampling error:

$$\hat{a}_t = a_t + \varepsilon_t \quad (\text{S.5})$$

Because of the sampling errors, the sample variance of the estimates \hat{a}_t is an upward-biased estimate of the true across-year variance in the parameter. That is undesirable if the model will be used to project how temporal variability affects population dynamics. However, maximum likelihood estimation gives us an approximate variance-covariance matrix \hat{V} of the sampling errors, V in the code above. With that information, we can estimate the parameters of a random effects model for the intercept parameters, and thereby improve the year-specific estimates and the estimate of the across-year variance.

The model is as follows. We make the standard mixed-models assumptions that the a_t are drawn independently from some fixed distribution with unknown variance σ^2 . We also assume that the estimates \hat{a}_t are unbiased, that is

$$\mathbb{E}(\varepsilon_t | a_t) = 0. \quad (\text{S.6})$$

920 These are optimistic assumptions, but not excessively optimistic. Some degree of tem-
 921 poral correlation will often be present, and as we explain at the end, it is theoretically
 922 possible to account for it. Maximum likelihood parameter estimates are not unbiased,
 923 but if the assumptions of maximum likelihood are satisfied the bias is asymptotically
 924 negligible compared to the standard error (the bias scales as the inverse of sample size,
 925 the standard error as the square root of the inverse of sample size).

926 Let S^2 denote the sample variance of the estimates \hat{a}_t . It can then be shown that

$$927 \quad \mathbb{E}(S^2) = \sigma^2 + \frac{1}{T} \sum_{t=1}^T \mathbb{E}Var(\varepsilon_t) - \frac{1}{T(T-1)} \sum_{i=1}^{j-1} \sum_{j=1}^T \mathbb{E}Cov(\varepsilon_i, \varepsilon_j). \quad (\text{S.7})$$

928 This is eqn. (1) in Gould and Nichols (1998) in our notation, without the term that results
 929 from temporal autocorrelation.

930 The terms besides σ^2 on the right-hand are the expected impact of sampling error
 931 on the across-year variance of the parameter estimates; their presence makes S^2 a biased
 932 estimate of σ^2 . However, all of those terms correspond to entries in the variance-
 933 covariance matrix V . We can therefore use our estimated variance-covariance matrix \hat{V}
 934 to remove the bias due to sampling variability:

$$935 \quad \hat{\sigma}^2 = S^2 - \frac{1}{T} \sum_{t=1}^T \hat{V}_{t,t} + \frac{1}{T(T-1)} \sum_{i=1}^{j-1} \sum_{j=1}^T \hat{V}_{i,j}. \quad (\text{S.8})$$

936 $\hat{\sigma}^2$ estimates the variance of the distribution from which the a_t are assumed to be drawn.

937 Using that estimate, we can adjust the year-specific estimates to reduce the ex-
 938 pected impact of sampling error. Depending on your purposes, there are two possible
 939 adjustments. The first option is the one used in the popular capture-recapture analysis
 940 software Mark Cooch and White (2020),

$$941 \quad \tilde{a}_t = \bar{a}_t + \sqrt{\frac{\hat{\sigma}^2}{\hat{\sigma}^2 + \hat{V}_{t,t}}} (\hat{a}_t - \bar{a}_t). \quad (\text{S.9})$$

942 The name “shrinkage” comes from the fact that each estimate is adjusted towards the
 943 overall mean, with larger adjustments of values that have higher estimated sampling
 944 error variance, $\hat{V}_{t,t}$. This shrinkage estimate has the property that the expected sample
 945 variance of the adjusted estimates \tilde{a}_t is very close to $\hat{\sigma}^2$, so the \tilde{a}_t approximate the actual
 946 amount of parameter variation.

947 The second is to replace \hat{a}_t by the least-squares estimate of a_t under the additional
 948 assumption that the a_t are drawn from a Gaussian distribution; this is given by

$$949 \quad \tilde{a}_t = \bar{a}_t + \frac{\hat{\sigma}^2}{\hat{\sigma}^2 + \hat{V}_{t,t}} (\hat{a}_t - \bar{a}_t). \quad (\text{S.10})$$

950 This option is theoretically preferable if the Gaussian assumption is reasonable, and you
 951 are more interested in year-specific values rather than across-year variance. However,
 952 Metcalf et al. (2015) found that even (S.9), which does less shrinkage, resulted in a small
 953 downward bias in the temporal variance of population growth rates. This argues for
 954 always using the first option, and we do the same here.

955 We differ from MARK, however, in using (S.8) rather than an iterative method
 956 that takes (S.8) as its starting estimate and refines the estimate by using weighted least
 957 squares based on the current estimate. Metcalf et al. (2015) found, in simulation studies,
 958 that the iterative method was either slightly beneficial or wildly inaccurate. We therefore
 959 advise against it.

960 Finally, as mentioned above, the estimate of σ^2 can account for temporal autocor-
 961 relation in the a_t . When present, those correlations add a term to eqn. (S.7) (see eqn.
 962 (1) in Gould and Nichols (1998)), which can be estimated from the sample autocorre-
 963 lation of the \hat{a}_t . We do not recommend doing this (and therefore omit the formulas)
 964 because the autocorrelations can only be reliably estimated if they fall to nearly zero
 965 within lag $m \ll T$, in which case the autocorrelation term is small (specifically, $O(m/T)$).
 966 Otherwise, the random error from using poorly estimated autocorrelations is likely to
 967 outweigh the small bias from omitting that term.

968 The take-home message is that estimating random effects from the regression coef-
 969 ficients is very simple:

```
970 # Variance-covariance matrices for intercepts and slopes
971 V1 = V[1:T,1:T]; V2 = V[(T+1):(2*T),(T+1):(2*T)];
972 # Extract year-specific intercepts, center them to zero
973 fixed.fx = coefs[1:T]; fixed.fx = fixed.fx-mean(fixed.fx);
974
975 # Estimate sigma^2
976 var.hat = mean(fixed.fx^2) - mean(diag(V1)) +
977           (sum(V1)-sum(diag(V1)))/(2*T*(T-1));
978
979 # Shrink deviations from the mean
```

```

980 shrinkRanIntercept = fixed.fx*sqrt(var.hat/(var.hat + diag(V1)));
981
982 # Do it all again for the slopes
983 fixed.fx2 = coefs[(T+1):(2*T)]; fixed.fx2 = fixed.fx2-mean(fixed.fx2);
984 var2.hat = mean(fixed.fx2^2) - mean(diag(V2)) +
985   (sum(V2)-sum(diag(V2)))/(2*T*(T-1));
986 shrinkRanSlope = fixed.fx2*sqrt(var2.hat/(var2.hat + diag(V2)));

```

987 The figure below shows the results for one artificial PSSP “data” set, having $T = 22$
988 years and growth measurements on about 175 individuals/year on average. The true
989 random year effects (the ones used to generate the data) are recovered with good accu-
990 racy and no bias. In particular there is no sign of extreme values being pulled in too
991 far towards the mean, which would cause an S-shaped graph of estimated versus true
992 values.

